

# AUSTRALIAN MUSEUM SCIENTIFIC PUBLICATIONS

Sutherland, F. L., and B. J. Barron, 1998. Balmoral Beach Aboriginal shell midden, Port Jackson, Australia: pumice petrology and sources. *Records of the Australian Museum* 50(3): 241–262. [25 November 1998].

doi:10.3853/j.0067-1975.50.1998.1284

ISSN 0067-1975

Published by the Australian Museum, Sydney

nature culture **discover**

Australian Museum science is freely accessible online at  
[www.australianmuseum.net.au/publications/](http://www.australianmuseum.net.au/publications/)  
6 College Street, Sydney NSW 2010, Australia



## **Balmoral Beach Aboriginal Shell Midden, Port Jackson, Australia: Pumice Petrology and Sources**

F.L. SUTHERLAND & B.J. BARRON

Geodiversity Research Centre, Australian Museum, 6 College Street, Sydney NSW 2000, Australia  
lins@ams.g.austmus.gov.au

**ABSTRACT.** Palaeopumice strand deposits (1800 to 4000 years B.P.) occur in the Balmoral Beach Aboriginal Shell Midden excavations. In composition, the pumice clasts are low-potassium dacites and contain up to 5% xenocrysts, phenocrysts and glomerophenocrysts of orthopyroxene, pyroxene, plagioclase and iron oxide minerals. The matrix includes smaller grains of these minerals in an abundant, highly vesicular rhyodacite volcanic glass. The 3300 year old and younger pumices typically contain rare xenocrysts and phenocrysts of magnesian olivine, forming an unusual mineral assemblage. One older pumice clast is a quartz-bearing rhyodacite, with distinctive trace element geochemistry. The typical dacites, resemble those erupted from the Tonga-Kermadec island arc in the Southwest Pacific, due both to the presence of olivine and the variably depleted trace and rare earth element contents. This implies a 4000 km drift caused by the East Australian oceanic current, before the pumice was stranded in Port Jackson.

SUTHERLAND, F.L., & B.J. BARRON, 1998. Balmoral Beach Aboriginal shell midden, Port Jackson, Australia: pumice petrology and sources. *Records of the Australian Museum* 50(3): 241–262.

Pumice regularly washes up on Australian coasts, usually after storm activity. In an early observation, Clarke (1842) remarked “An investigation of the range of this drift pumice along the shores of Australia and Tasmania would not be an unimportant employment”. Since then, a few studies identifying pumice sources have been made. One major pumice stranding in southern Australian coasts and sub Antarctic islands, starting in late 1963, was traced to a 1962 submarine eruption in the South Sandwich Islands over 8000 km away (Sutherland, 1965; Coombs & Landis, 1966). This pumice dispersed on the southern polar currents may have even circumnavigated the Southern Ocean to restrand as fine pumice gravel on Australasian coasts by mid-1965 (Sutherland & Olsen, 1968). More recently, studies of pumice stranded on cays and beaches along North

Queensland have suggested Southwest Pacific sources, mostly from the Tonga-Kermadec island arcs some 4000 km away (Bryan, 1968; Stanton, 1992). This pumice travels on the South Equatorial Current, east to west from Fiji to the Coral Sea. Here the current splits and the main branch runs north to south along the Australian shelf deflecting off southern New South Wales to run from west to east (Rotschi & Le Masson, 1967; Tomczak & Hao, 1989; Burrage, 1993). Thus, Southwest Pacific sources could be expected to supply a large proportion of the pumice washing up on New South Wales coasts (Fig. 1). Extended sources could be involved as the tropical convergence separating the east to west flowing South Equatorial Current from the returning west to east currents ranges from 18–25°S (cf. Martinez, 1994, and Nelson *et al.*, 1994).

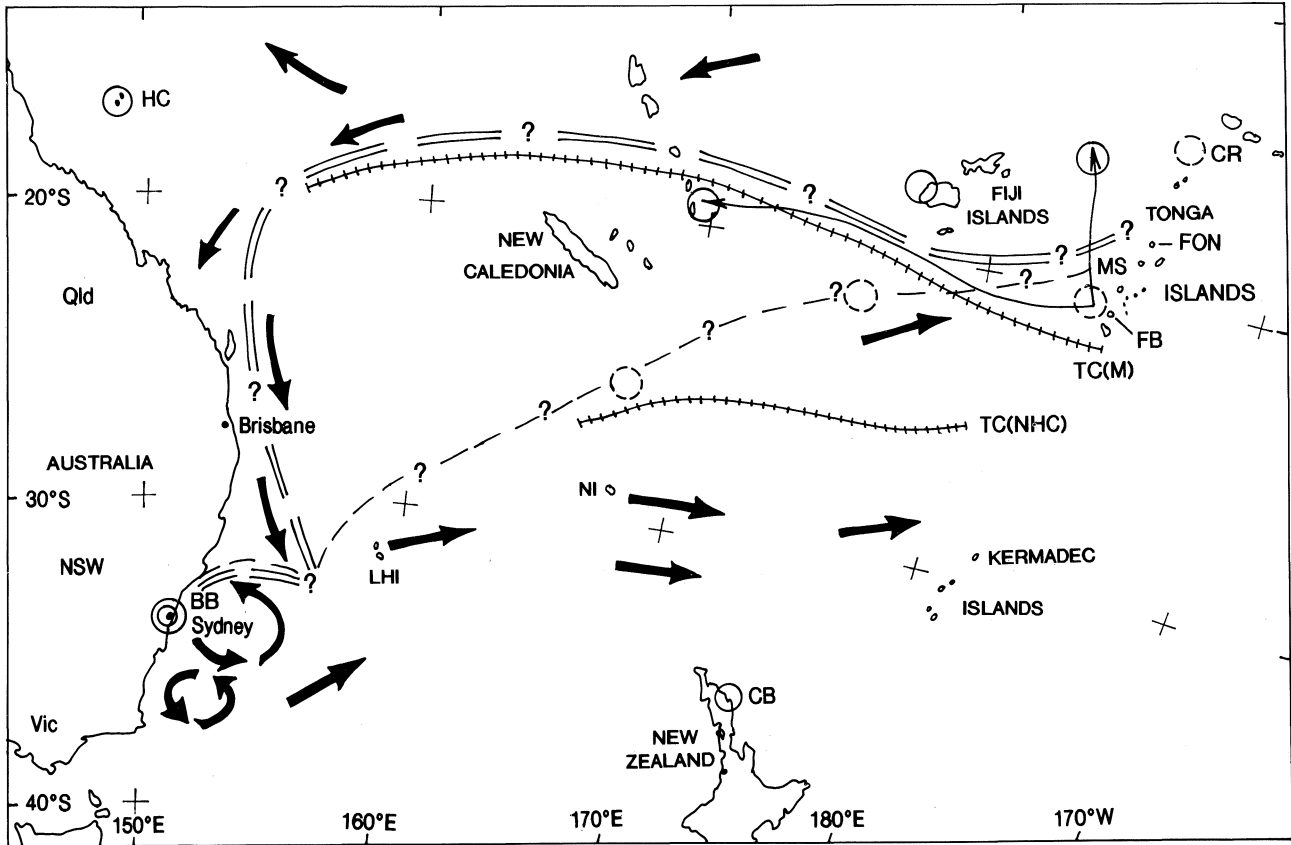


**Figure 1.** Map of eastern Australia-southwestern Pacific region after Bryan (1968), showing locations of pumice sightings (dashed circles) and pumice strandings (complete circles), with the 1928 Falcon Bank (FB) pumice eruption sites linked by thin arrowed lines and Balmoral Beach (BB) palaeopumice site indicated by double circle. Other sites include Fonualei dacite volcano (FON), Metis Shoal (MS) Curaçoa Reef (CR), Herald Cays (HC), Cape Brett (CB), Norfolk Island (NI) and Lord Howe Island (LHI). The two positions shown for the Tropical Convergence (hatched lines) follow Martinez (1994), symbolised TC (M), and Nelson *et al.* (1994), symbolised TC (NHC). Main surface current flow directions are indicated by heavy arrows, while two alternative routes for Balmoral pumice drift from a potential North Tongan source are indicated by double dashed and single dashed lines.

Major submarine pumice eruptions occur repeatedly from the Tonga-Kermadec volcanic arc and the pumice usually drifts through Fiji and New Caledonia before reaching East Australian coasts about a year later (Jokiel, 1990). These eruptions not only introduce exotic pumice onto Australian coasts, but the pumice also transports exotic coral juveniles from far east and south east regions into the Great Barrier Reef off Queensland, which helps to build up the coral diversity. The many submarine pumice eruptions from island arcs bounding the eastern Australian plate margin combined with the prevailing east to west current flows from these regions produce the considerable range of pumice compositions found within Australian Holocene beach deposits (e.g., south eastern Queensland coasts; Little & Ward, 1980). The ability of Southwest Pacific pumice to travel considerable distances is documented by drift pumice from a submarine Tonga Trench eruption appearing in the Indian-South Atlantic Ocean region (Frick & Kent, 1984). Catastrophic caldera pumice eruptions are also recorded in the last 4000 years

from the North New Zealand-Kermadec-Tonga volcanic zone (Taupo, New Zealand [Pullar *et al.*, 1977]; Raoul Island [Lloyd & Nathan, 1981]); these can release large quantities of sea-rafted pumice. Some of these sea-borne pumices could reach Australian coasts, depending on past current patterns.

As well as historic pumice strandings, pumice layers also appear in prehistoric Holocene raised beach deposits on eastern Australian coasts, e.g., North Bulli raised beach deposits at 4 m a.s.l. dated at  $5200 \pm 2000$  years (Bryant *et al.*, 1992a). Profuse pumice also appears in later disturbed beach deposits, interpreted as possible tsunami effects in the last 3000 years (Bryant *et al.*, 1992b). However, petrological studies and detailed sources for such pumices are not yet reported. Archaeological excavations at the Balmoral Beach Aboriginal midden site within and outside a rock shelter in Port Jackson, revealed pumice-bearing layers within the sequence dated between 1800 to 4000 years B.P. The main pumice layers were dated at  $3280 \pm 60$  B.P. and  $3250 \pm 90$  B.P. using radiocarbon determinations

on associated charcoal and these layers lie close to present sea level (Attenbrow *et al.*, 1997; Attenbrow & Hashimoto, in prep.).

This paper describes the petrology of pumice pieces sampled from the main pumice horizon and from sparser pumice in horizons below and above this main pumice horizon.

### Analytical methods

Pumice pieces were sectioned for microscopic examination and analysis of contained crystals and glass matrix. From this analytical base, comparisons were made with pumices of similar petrology described in the literature, particularly pumice described from Southwest Pacific regions, to suggest potential sources.

Seven pumice samples were examined. P1, P2 and P5 came from the main 3300 year old pumice layer, with P1 and P5 coming from outside the rock shelter and P2 from inside the rock shelter. P3, P6, P7 came from lower, earlier levels in both sites that are dated between 3300 and 3500 years, while P4 came from higher later levels dated between 1800–2800 years.

Pumice samples were viewed under a stereo-microscope and polished thin sections of selected pieces were studied using a polarising petrological microscope, prior to electron microprobe (EMP) analysis. Compositions of mineral grains and glassy matrix were made on a CAMECA S X 50 Microprobe, at Macquarie University, Sydney, using an accelerating voltage of 15 kV and a beam current of 20 na, measured in a Faraday cup. Precisions were better than  $\pm 1\%$  for elements over 10 wt% oxide,  $\pm 5\%$  at 1–10 wt% levels and  $\pm 10$  at levels below  $\pm 1$  wt%. Bulk whole rock analyses of pumice were not attempted due to uncertainties of contamination and leaching effects in the more altered glass. However, approximate bulk analyses were calculated by combining mineral mode compositions with fresh glass analyses.

Trace elements, including Rare Earth Elements (REE), were analysed from four pumice glasses using laser ablation and Induced Coupled Plasma Mass Spectrometry (ICPMS) at Macquarie University, Sydney (Norman *et al.*, 1996). The laser source used a Continuum Surelite I-20Nd:YAG laser, with wavelength 266 nm, Q-switch delay of 230  $\mu$ sec., frequency of 2 Hz, power of 2 mW and energy of 1 mJ/pulse. The ICP-MS used a Perkin Elmer ELAN 5100 spectrometer, with a peak hop scanning mode, 50 msec. dwell time, 1 sweep/reading and between 20–60 replicate analyses. The Calibration Standard was NIST 610 glass and the Internal Standard was Ca44. The accuracy in element values increases with count time, so that the lower count times were not considered among the final analyses used for plotting results.

### Pumice description

Features of the samples P1 to P7, their mineral contents and glass type are summarised in Table 1 and hand specimen and polished, thin-section descriptions of the

pumice samples can be obtained from the authors. All pumices include mineral xenocrysts, phenocrysts and glomerophenocrysts that make up between 1–5 volume percentage of the rock. Minerals commonly include plagioclase, clinopyroxene, orthopyroxene and opaque iron oxides, but four of the seven pumices contain olivine (P1, P2, P4, P5) and one olivine-free pumice contains phenocrystic quartz (P7). Olivine and clinopyroxene appear in both xenocryst and phenocryst forms (Figs. 2, 3) and glomeroporphyritic groups commonly contain pyroxenes (Fig. 4) and plagioclase (Fig. 5). Some phenocrysts show magmatic corrosion, inclusions of glassy melt and intergrowths with opaque oxides and even apatite (Fig. 6). Quartz microphenocrysts appear in only one sample (Fig. 7).

Pumice clasts are generally extensively vesiculated, with voids forming 60–80% of the rock. In some pieces voids show changes in flow alignment and flattening, suggesting aggregates of spatter (Fig. 8). The pumice may be partially altered making refractive index determinations of matrix glass problematical. However, all fresh glasses analysed by EMP were silica-rich in the range of rhyodacite-rhyolite (71–77 wt% SiO<sub>2</sub>). Most pumices contain a range of xenocryst/phenocryst minerals, with plagioclase (50–55%) dominating over orthopyroxene (15–30%) and clinopyroxene (10–20%), and opaque oxides (10%) and olivine (2–5%) forming accessory roles. However, P3 is dominated by orthopyroxene and clinopyroxene phenocrysts with only sparse plagioclase and oxides.

### Analytical results

Representative compositions of pumice minerals for P1, P4–7 are given in Table 2 and are plotted in standard chemical variation diagrams in Fig. 9.

**Mineral compositions.** Calcian plagioclase dominates phenocrystic feldspar in most pumices (Fig. 9A). Zoning in some phenocrysts trends from calcian (core) to more sodian (rim) compositions. Microphenocryst and groundmass compositions as calcian as bytownite appear in one pumice (P6), while xenocrysts and phenocrysts as sodian as andesine associated with a labradorite-bearing groundmass appear in another (P1).

Orthopyroxene compositions are moderately iron-rich (Mg<sub>50–60</sub> Fe<sub>35–40</sub> Ca<sub>0–5</sub>). Clinopyroxenes include both diopside and augite (Fig. 9B) and both can occur together (P2, P5). The diopside shows zoning from more magnesian cores to more iron-enriched rims and olivine shows two distinct compositions (P1, P2; Fig. 9B). A xenocryst/resorbed phenocryst (Fig. 9C) of magnesian olivine (Fo<sub>89–91</sub>) contrasts with more iron-enriched phenocrystic olivine (Fo<sub>82–83</sub>).

Opaque iron oxides are dominated by members of the magnetite-ulvospinel series and include near end-member magnetite and two titanian ulvospinel phases (Fig. 9D). The main layer pumices (P1, P2, P5) contain both magnetite and the more titanian ulvospinel and minor ilmenite, while other pumices typically contain an intermediate titanian ulvospinel.

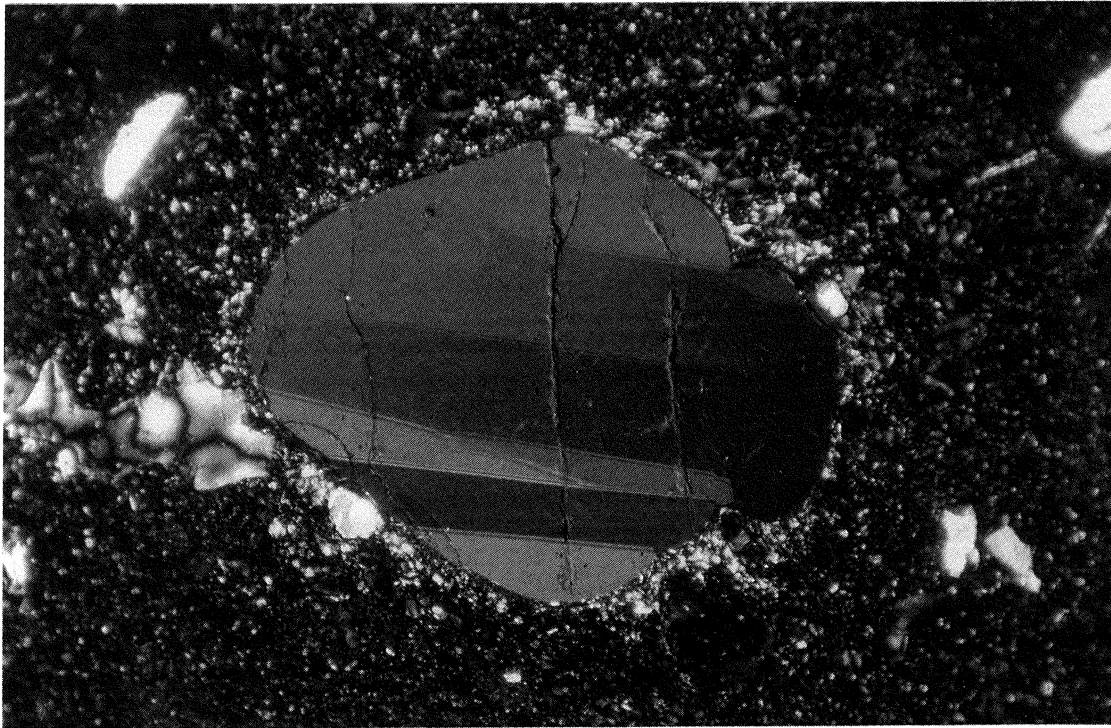


**Figure 2.** Olivine xenocryst (1 mm long) showing strain lamellae in vesicular volcanic glass (Pumice P1). Cross polarised light. (Photomicrography—B.J. Barron).

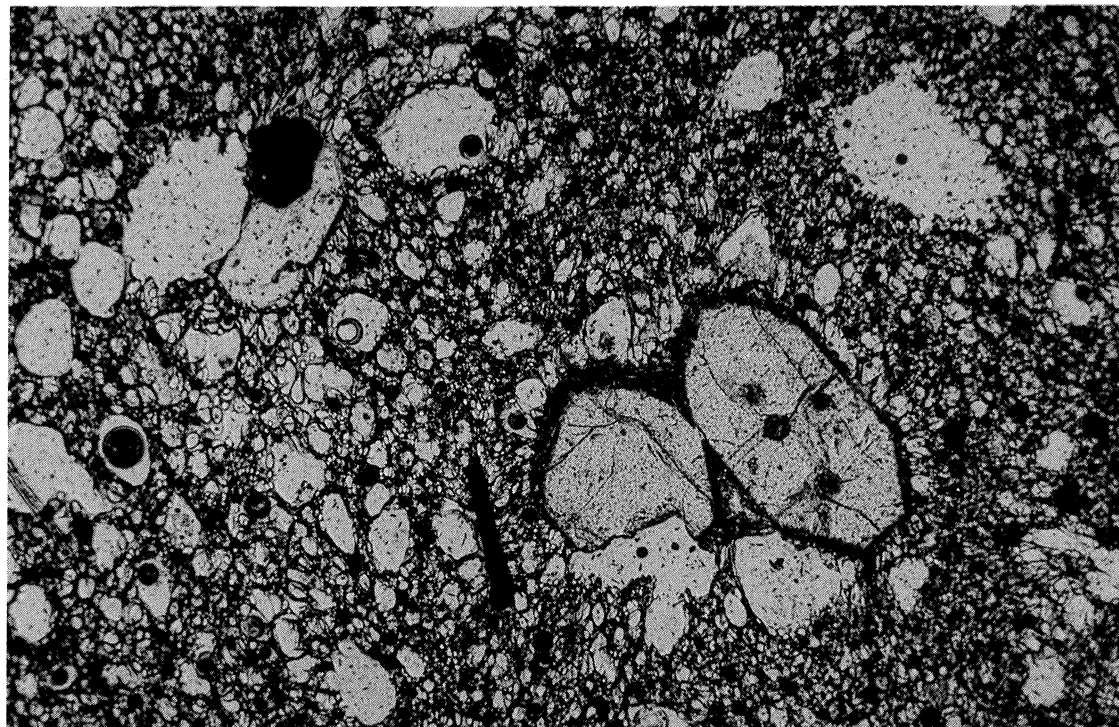


**Figure 3.** Olivine phenocrysts (up to 0.5 mm long) and small plagioclase-opaque iron oxide glomerophenocryst in vesicular volcanic glass (Pumice P2). (Photomicrography—B.J. Barron).

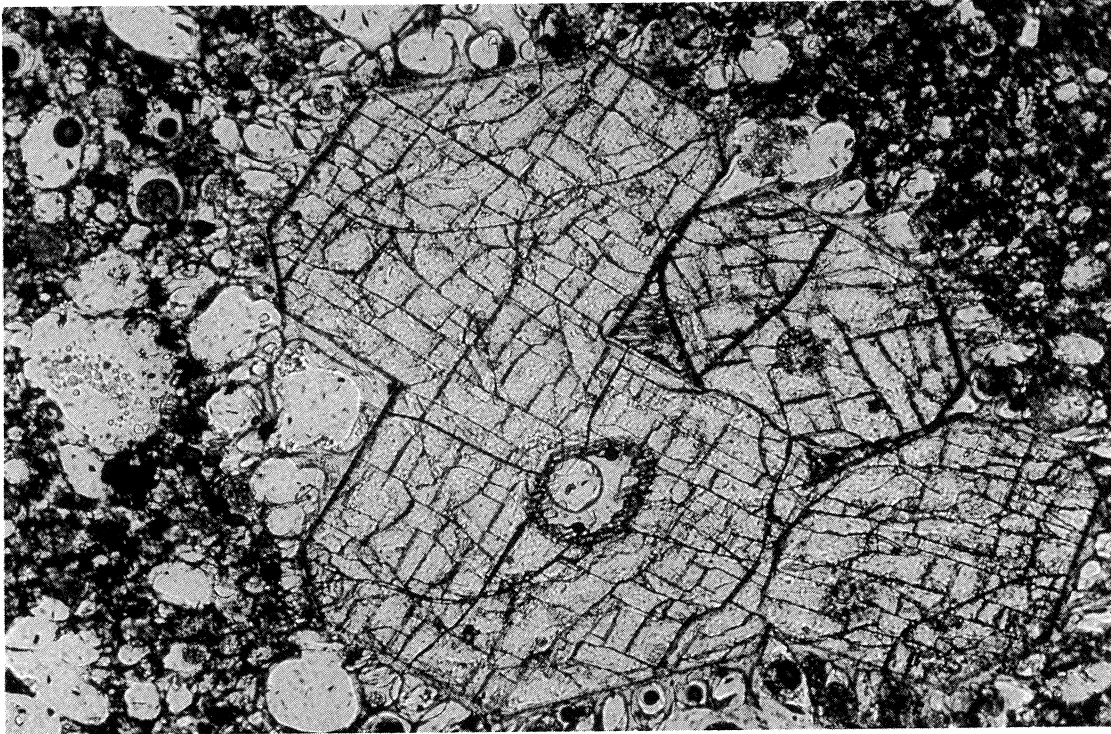


**Figure 4.** Clinopyroxene glomerophenocrysts in vesicular volcanic glass (Pumice P1). The largest double crystal (0.6 mm across) contains a rounded volcanic glass inclusion with a rim of minute amphibole(?) crystals. Plane polarised light. (Photomicrography—B.J. Barron).

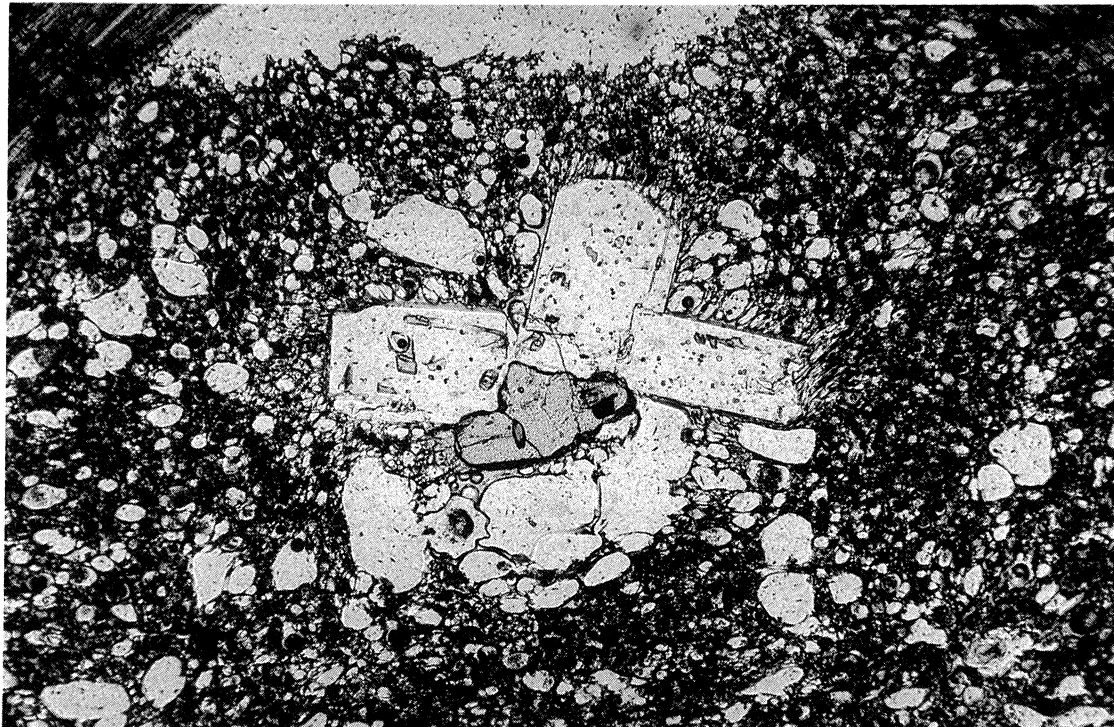


**Figure 5.** Plagioclase glomerophenocrysts (cluster 0.8 mm across) surrounding a pale green orthopyroxene crystal (0.3 mm long) in an intensely vesicular volcanic glass (Pumice P1). The plagioclase crystals contain fluid inclusions and the orthopyroxene crystal contains an inclusion of brown volcanic glass and an opaque oxide. Plane polarised light. (Photomicrography—B.J. Barron).

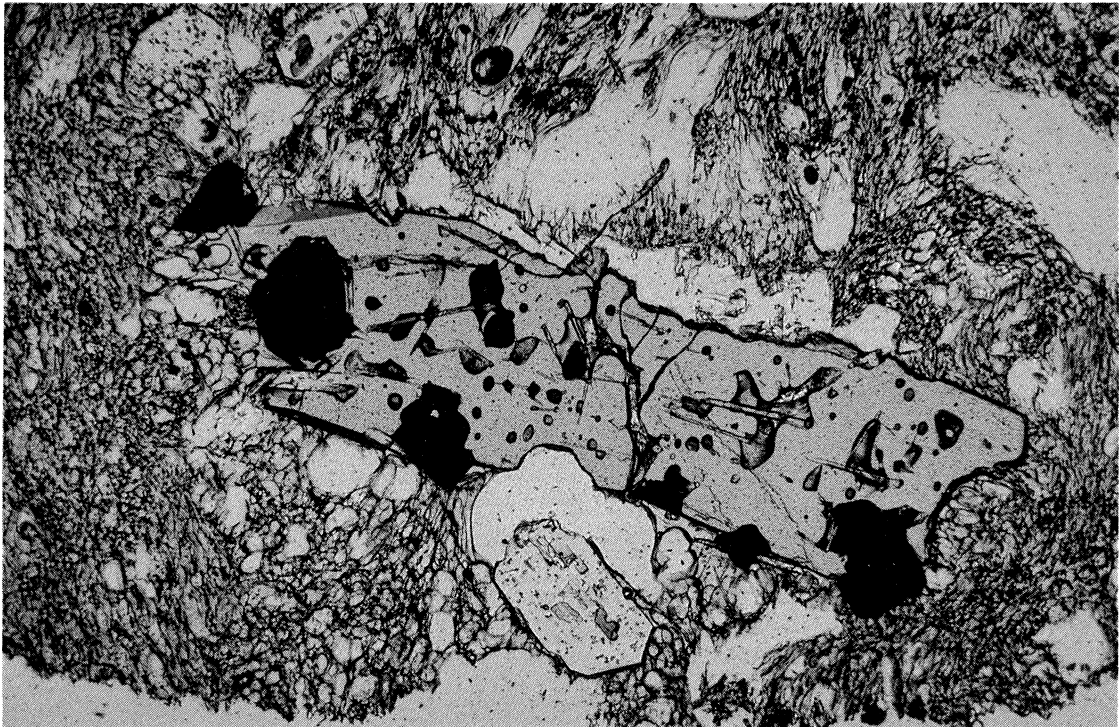


**Figure 6.** Orthopyroxene phenocryst (1.4 mm long) in vesicular volcanic glass (Pumice P5). The pale green orthopyroxene crystal is somewhat corroded and encloses abundant inclusions of opaque iron oxide, apatite needles and pale brown volcanic glass. Plane polarised light. (Photomicrography—B.J. Barron).

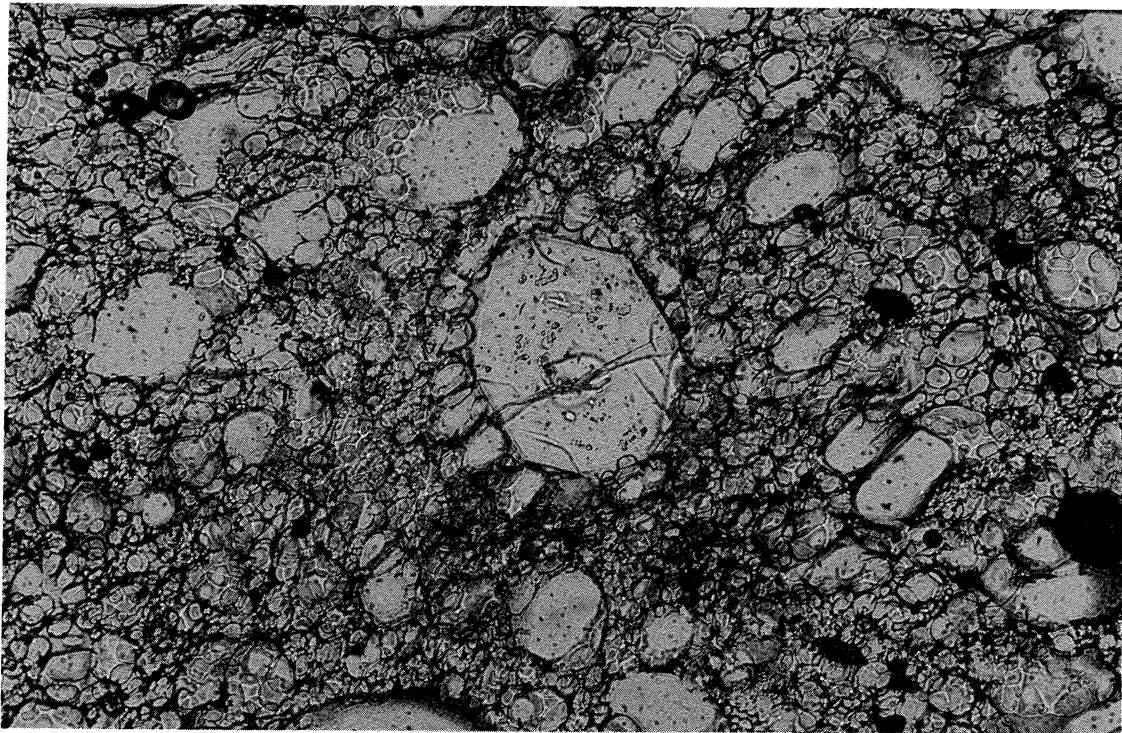


**Figure 7.** Quartz phenocryst (0.2 mm long) in intensely vesicular volcanic glass (Pumice P7). Part crossed polarised light. (Photomicrography—B.J. Barron).

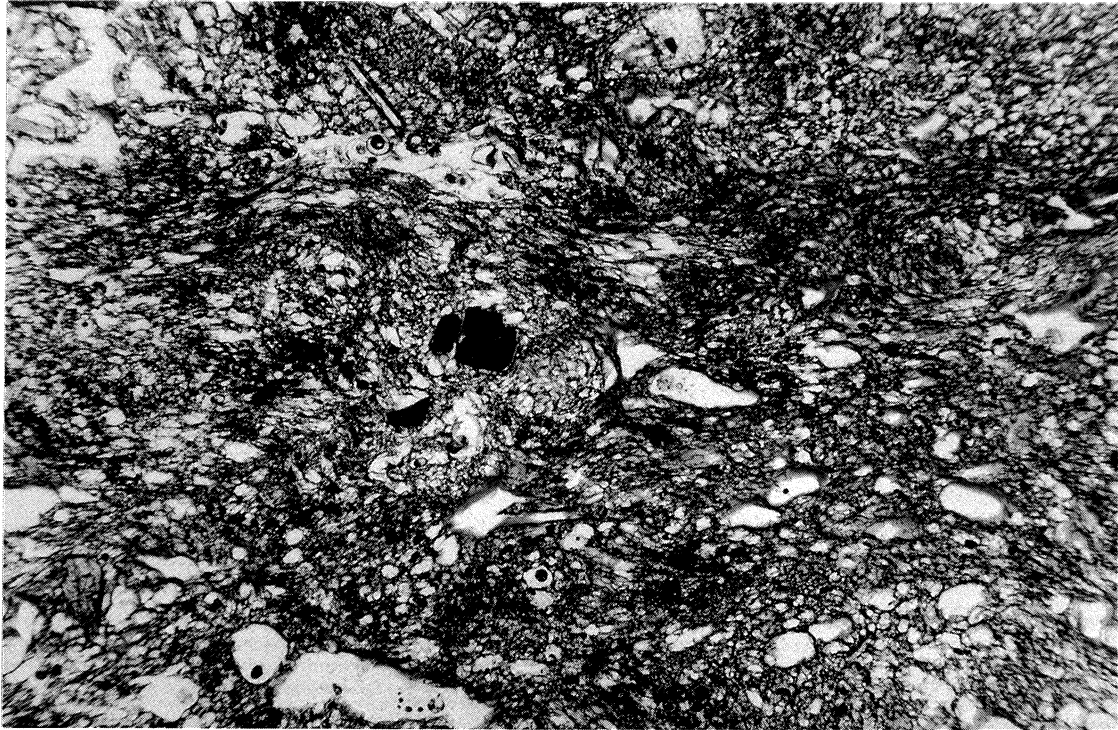


**Figure 8.** Vesicular volcanic glass (Pumice P3) showing somewhat chaotic eutaxitic texture and partial oxidation from weathering. The field of view is 2.8 mm in long dimension. Plane polarised light. (Photomicrography—B.J. Barron).

**Glass compositions.** Representative glass compositions for pumice matrix fractions and for glass included in pyroxenes are presented in Table 3, with their calculated anhydrous CIPW norms. All glasses are silica-rich, with low alkalis and relatively sodic compositions. They are quite rich in normative calcian plagioclase and also show minor normative corundum. Glass inclusion compositions overlap matrix glass compositions and form trapped melt. All glasses represent evolved melts, ranging from D.I. 67–75 and Mg number 18–28 (Table 3) and showing high normative quartz (Fig. 9E). They pass into rhyodacitic compositions (over 69 wt% SiO<sub>2</sub>; Wilson, 1989). The appearance of quartz and corundum together in the norm probably reflects low alkalis (Hughes, 1982: 101), so that all calcium is combined with aluminium to form plagioclase. This would leave insufficient calcium to form normative diopside, present in small amounts in other comparable rhyolitic glasses (0.6–3.3% di; Table 3).

**Trace elements.** These were determined on matrix glass from four pumice samples and as the glass is 4 to 5 times more abundant than the phenocrysts the analyses provide useful signatures to characterise pumice differences. Representative laser ablation ICP-MS results for Large Ion Lithophile (LIL), High Field Strength (HFS) and Rare Earth (RE) elements are listed in Table 3 and their chondrite-normalised patterns are compared in Fig. 10.

All patterns show spiked profiles predominantly with values enhanced compared to the chondritic mantle, following chondrite values used by Taylor & McLennan

(1985). A notable trough is present for Nb relative to Zr in the HFS elements and peaks for Ba and U appear in the LIL elements. The REE patterns are relatively flat and a noticeable Eu depletion only appears in the main layer pumice (P2). Each pattern however is distinctive, showing variation in Th, Sr, Nd, Hf, Pr, Y and Pb enrichments and depletions. The quartz-bearing pumice (P7) is markedly different, in its relatively higher Rb, Th, Pr and Pb.

### Pumice characterisation

The pumices contain rhyodacitic glass (over 69 wt% SiO<sub>2</sub>) as their major component. However, these residual compositions do not reflect their bulk compositions, as these will be modified by the xenocryst/phenocryst contents. Bulk analyses of pumices were not made, as alteration in the pumices would lead to misleading results. However, approximate bulk major element compositions can be estimated by combining the remnant fresh glass composition with mineral compositions of the included crystals. Calculated bulk compositions for pumice samples P1 and P2 in the main pumice layer are given in Table 5. Relative to K<sub>2</sub>O, these show a general decrease in SiO<sub>2</sub> and increases in FeO (total), CaO and MgO, with relatively minor increases in Al<sub>2</sub>O<sub>3</sub> and in Na<sub>2</sub>O. The estimates of the bulk compositions correspond to low-potassium dacites (63–69 wt% SiO<sub>2</sub>).

The pronounced Nb depletion relative to Zr and strong Ba and U enrichment in the chondrite-normalised trace

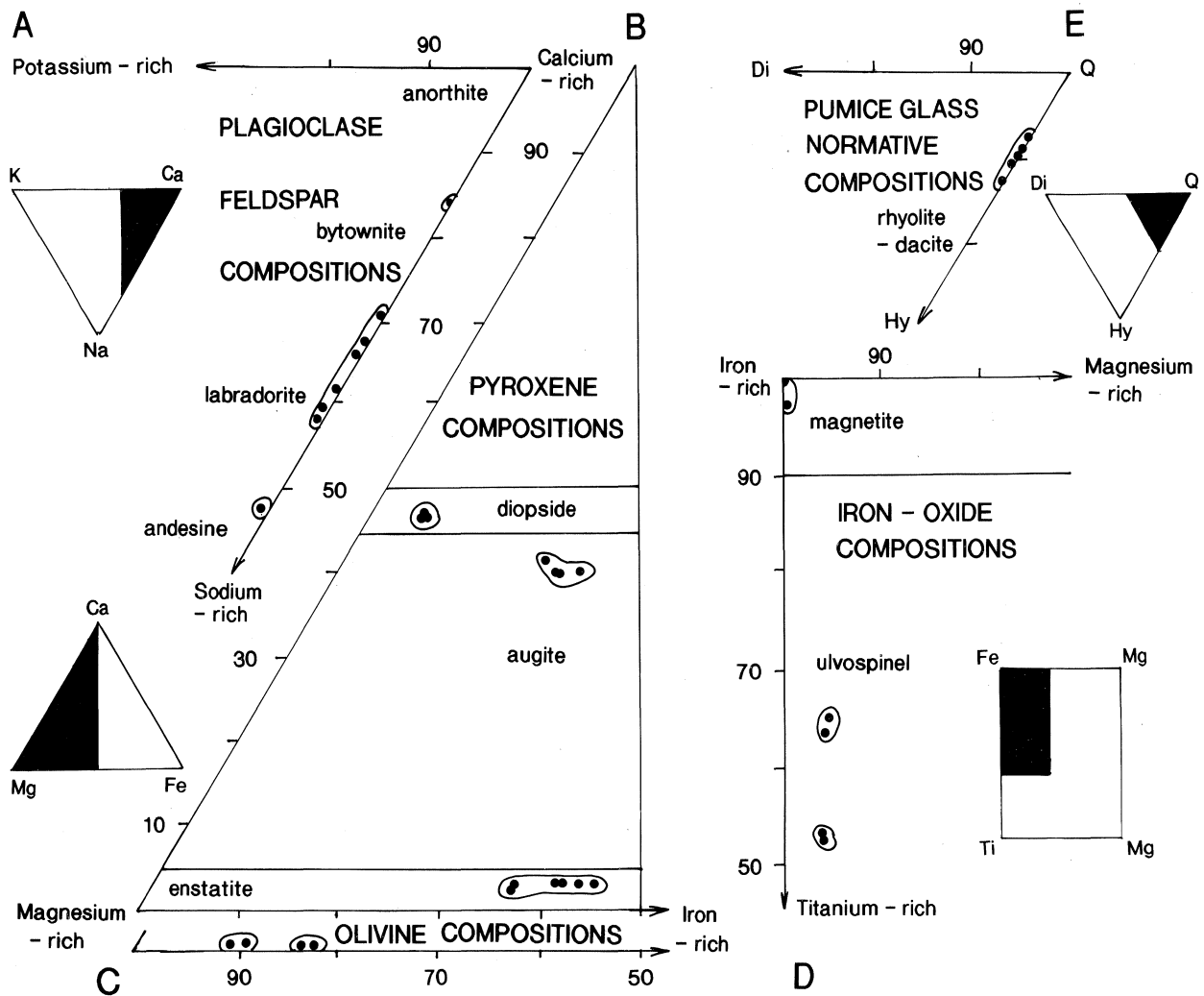


**Figure 9.** Mineral and glass composition plots (solid dots within circled fields) for Balmoral Beach pumices, with mineral cation data taken from Tables 2A–2D and normative glass data from Table 3. A, plagioclase feldspar compositions plotted in a Ca-Na-K triangular diagram; B, pyroxene cation plots in an Mg-Ca-Fe triangular diagram; C, olivine cation plots in an Mg-Ca-Fe triangular diagram; D, iron oxide cation plots in an Fe-Mg, Fe-Ti, quadrilateral diagram; E, normative pumice glass plots in a di-qz-hy triangular diagram. Note the plots do not include potential small diopside components, due to possible minor deficiencies in alkalis.

elements in the pumice glasses are features typical of island arc rocks (Wilson, 1989: 172–180). However, low alkalis are characteristic, especially potassium, in Balmoral pumices. The low-K presumably is linked to the depleted Rb and sometimes Sr found in these glasses. Such low-K dacites, rhyodacites and rhyolites, lacking hydrous phenocryst phases, are typical of evolved rocks erupted from the Tonga-Kermadec island arc (Melson *et al.*, 1970; Bryan *et al.*, 1972; Ewart & Bryan, 1973; Ewart *et al.*, 1973, 1977; Bryan, 1979; Ewart & Hawkesworth, 1987) and are also found among glasses in the Lau Basin volcanoclastic record since 5 Ma (Clift & Vroon, 1996). These features also characterise drift pumice that reaches the east Australian coast (Bryan, 1968) and comparative trace element and bulk analyses of the Balmoral pumice, Coral Sea drift pumice, Tongan dacites and Lau Basin rhyodacitic glasses are given in Tables 4 and 5.

Temperatures of crystallisation for early phenocrystic, olivine and diopside in pumices P1 and P2 were calculated from their mineral compositions, using the newly developed olivine-clinopyroxene geothermometer of Loucks (1996). These give temperatures between 980–1040°C which overlap with those determined for Tongan basaltic andesites from pyroxene equilibration thermometry (992–1125°C; Ewart *et al.*, 1977). The calculated temperatures, however, may not directly relate to the host dacite, as these phenocrysts may be basaltic in origin; many Tonga-Kermadec arc felsic magmas contain phenocryst assemblages that can be interpreted as resulting from accidental inclusion of basaltic crystals (I.E.M. Smith communication, 1997). Co-existing pyroxenes in pyroxene-plagioclase glomerophenocrysts (pumice P2) give temperatures between 890–960°C (Fe<sup>3+</sup> recalculated compositions) based on two-pyroxene thermometry of

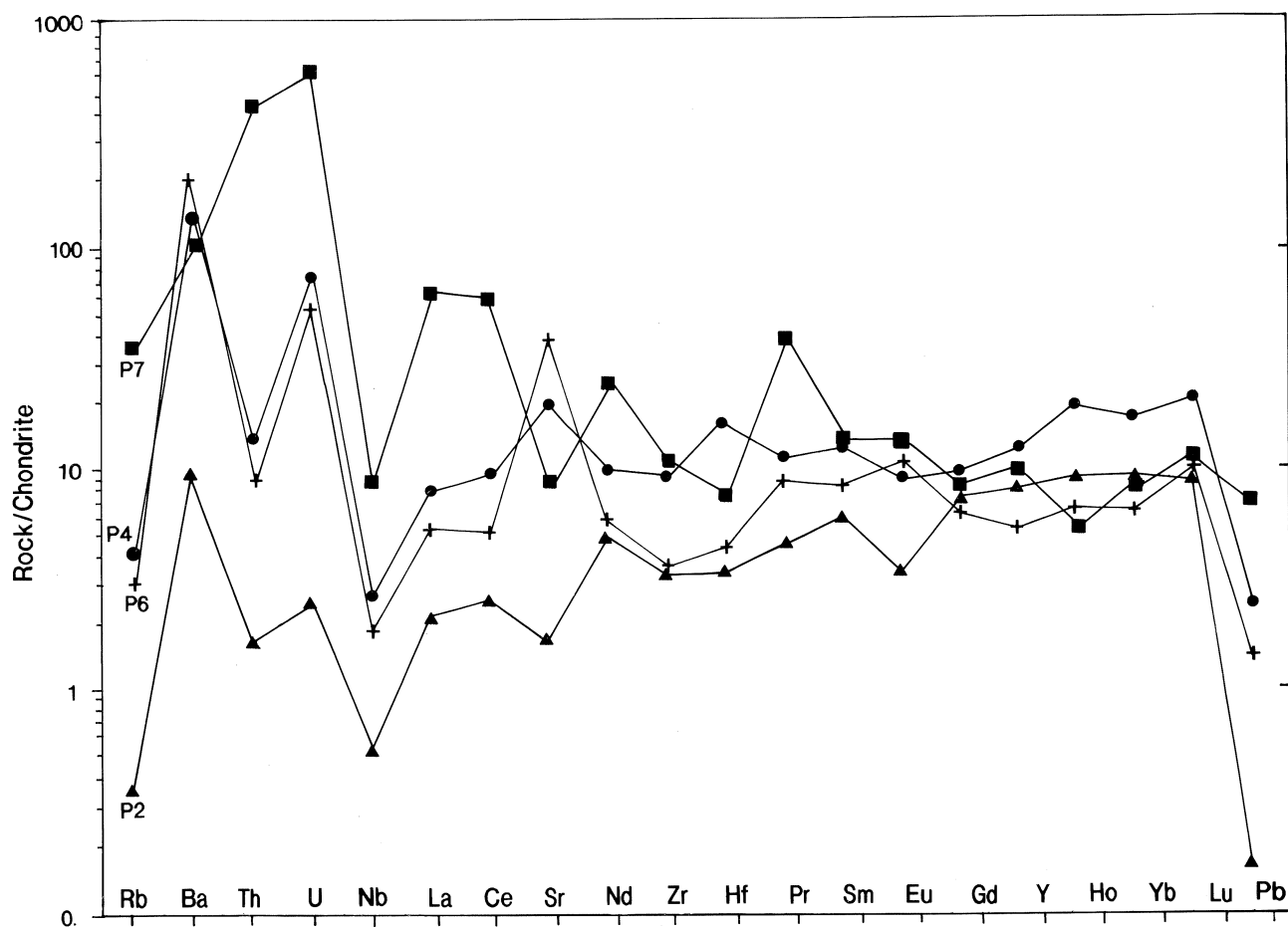


**Figure 10.** Incompatible and rare earth trace element chondrite-normalised plots (chondrite values after Taylor & McLennan, 1985) for representative pumice pieces, with P2 (triangles) from main pumice layer, P4 (solid dots) from later pumice layers and P6 (crosses) and P7 (solid squares) from earlier pumice layers. Trace element values normalised from Table 4.

Wood & Banno (1973) and Wells (1977) and these lie in the temperature range of 764–1150°C estimated for Tongan dacites from plagioclase thermometry at water pressures between 1–5 kb (Ewart *et al.*, 1973).

An unusual feature of pumices from the main and later layers (P1–2, P4–5) is the presence of xenocrysts/phenocrysts of magnesian olivine associated with a rhyodacitic glass. This characteristic is recorded in the Southwest Pacific area only from the Tongan islands, e.g., Metis Shoal (Melson *et al.*, 1970), so the 3300 year old and later Balmoral pumices may have originated from this region.

### Discussion

The general similarities in phenocryst mineralogy and glass compositions for much of the Balmoral pumice suggests they came from a related source region. Low alkalis, with low  $K_2O$  are typical of Tonga-Kermadec arc rocks, although the Balmoral pumices seem particularly poor in alkalis (Table 6). Some alkalis may have preferentially volatilised during EMP analysis of the Balmoral glasses,

as sodium loss can occur (Reed, 1975: 182–185). However pronounced loss is unlikely in this case, with use of a defocused beam. The low Rb and incompatible elements in most of these glasses suggests that any K loss was relatively limited. The rare quartz-rhyodacite pumice (P7) from pre-3300 year levels shows a distinctly different trace element pattern to the other rocks, which may reflect a separate source region. This pumice glass has the highest  $K_2O$  (1 wt%) and has significantly lower K/Rb (29.5), higher Rb/Sr (0.83) and greater Ce (111 ppm), La (84 ppm) and Zr (178 ppm) contents than observed in the other pumices. In these characteristics it resembles rhyolites and dacites that are erupted through continental crust, as in North Island, New Zealand, (K/Rb < 270, Rb/Sr > 0.2; Ewart *et al.*, 1973, 1977).

**Tongan Arc sources.** The discrimination between potential Tongan or Kermadec sources for most Balmoral pumices is somewhat problematical. Tongan dacites are generally enriched in iron relative to alkalis compared to Kermadec dacites (Ewart *et al.*, 1977). Thus, Balmoral dacites appear closer to the Tongan field (Fig. 11). However, the Metis

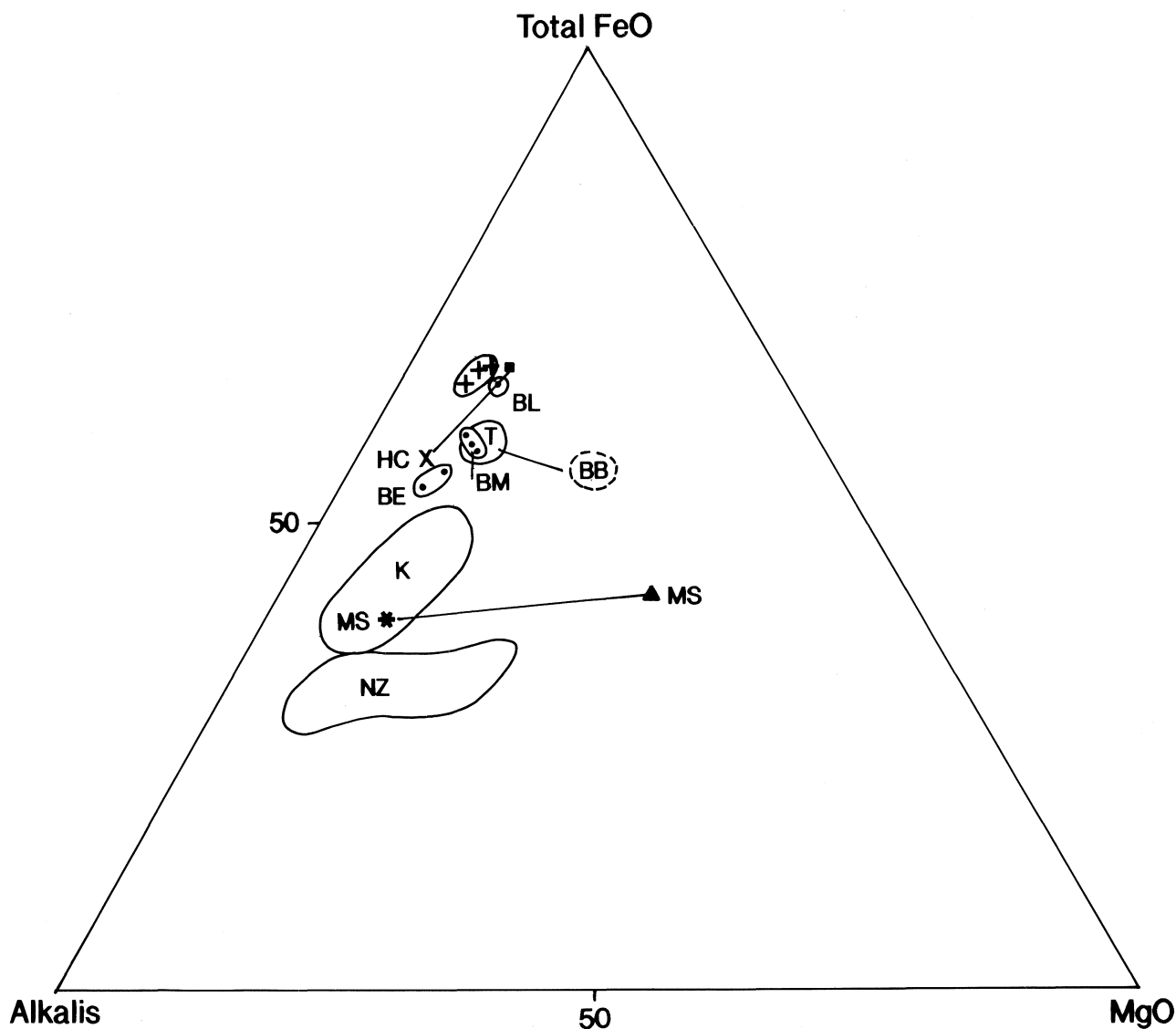


**Figure 11.** Total alkalis ( $\text{Na}_2\text{O}+\text{K}_2\text{O}$ )-FeO-MgO wt% variation diagram, showing plots of Balmoral Beach, Herald Cays and Metis Shoal dacite compositions in relation to Tonga (T), Kermadec (K) and New Zealand (NZ) dacite fields. Balmoral Beach bulk compositions (BB dashed field) connected to Balmoral main pumice glass compositions (BM enclosed dots), Balmoral later pumice glass composition (BL enclosed dot), Balmoral earlier pumice glass compositions (BI enclosed crosses), Herald Cays dark (square) and light (inclined cross) pumice compositions (HC tie line), Metis Shoal bulk (triangle), and glass (star) pumice compositions (MS tie line). Compositions from Tables 3, 5 and 6 and Southwest Pacific-New Zealand dacite fields from Ewart *et al.* (1977).

Shoal dacite and glass from Tonga plot near the Kermadec field (Ewart *et al.*, 1973). Also, any loss of alkalis from Balmoral glasses during EMP analysis, would shift plots towards the Kermadec and Metis Shoal fields.

Ewart & Hawkesworth (1987) plotted  $\text{Al}_2\text{O}_3/\text{TiO}_2$  against  $\text{CaO}/\text{TiO}_2$  and showed that, providing plagioclase accumulation effects were compensated for, both  $\text{Al}_2\text{O}_3/\text{TiO}_2$  and  $\text{CaO}/\text{TiO}_2$  decreased systematically along the arc from north Tonga to south Kermadec. Plots of Balmoral compositions are compared with plots from Fonualei Island and Metis Shoal, Tonga, from the Kermadec islands and from other east Australian low-K drift pumice in Fig. 12;

note that these above oxide ratios will not be affected by any potential loss of alkalis from the Balmoral analyses. The Metis Shoal bulk analysis, with some 9% plagioclase phenocryst content, is well separated from its glass composition. However, compensation for any plagioclase accumulation effects would shift compositions towards the glass plots. Balmoral pumices contain much less plagioclase phenocrysts (2–3%) and the estimated bulk plots lie closer to the glass plots. This suggests that the bulk plots would require little adjustment for plagioclase accumulation. When plagioclase compensation trends are applied to the Tongan and Kermadec dacitic fields, similar

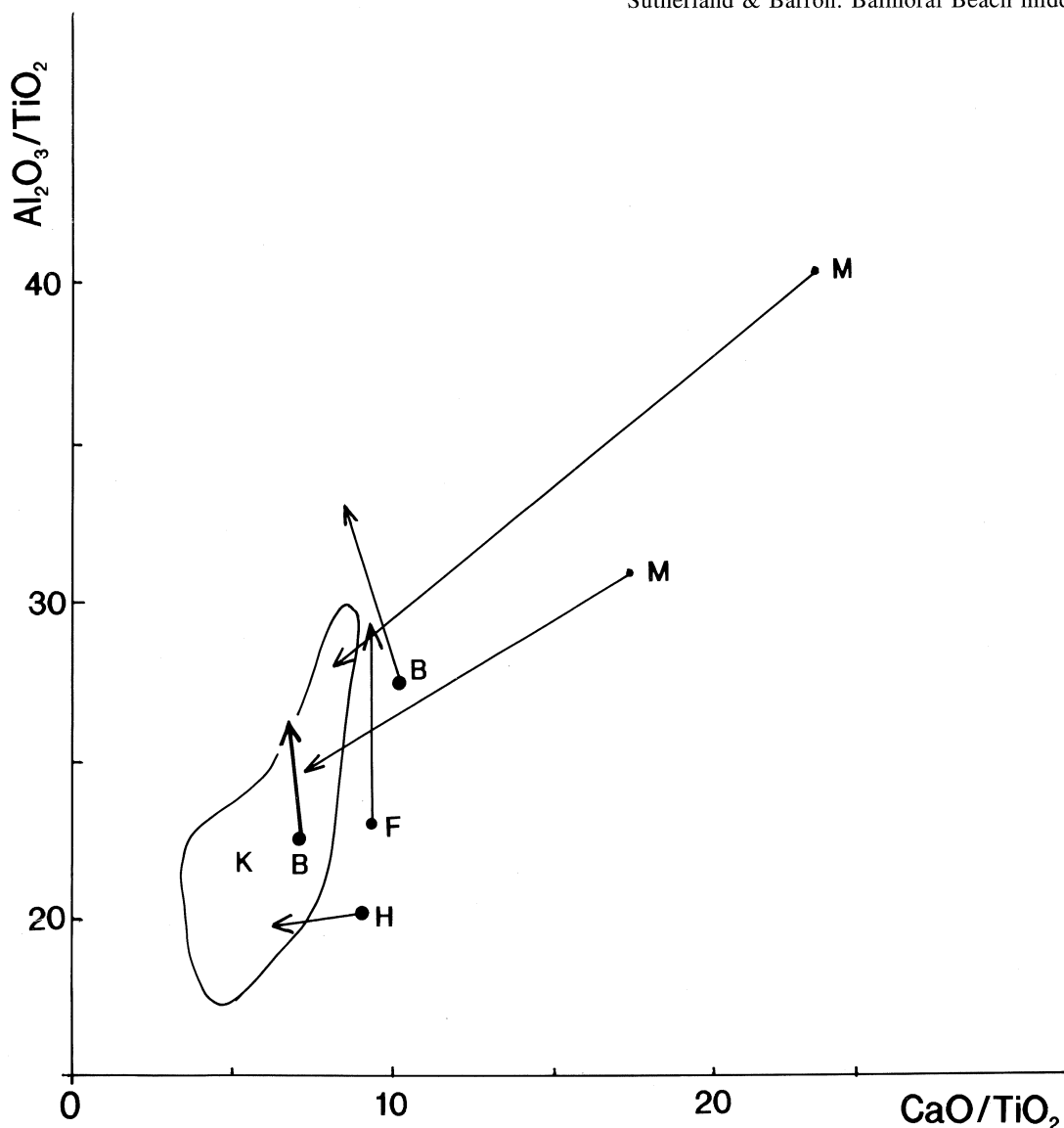


**Figure 12.**  $\text{Al}_2\text{O}_3/\text{TiO}_2$  versus  $\text{CaO}/\text{TiO}_2$  wt% variations diagram, showing trends for Balmoral Beach main pumice calculated bulk and glass compositions (B heavy dot arrow), Metis Shoal bulk dacite and glass composition (M light dot arrows), Fonualei bulk dacite and matrix composition (F light dot arrow), Herald Cays dark and light pumice compositions (H light dot arrow), in relation to Kermadec dacite field (K). Data from Tables 3, 5 & 6, with Kermadec dacite field based on analyses from Ewart *et al.* (1977).

to those for the basalt and basaltic andesite fields, then Balmoral glasses plot closer to Tongan than Kermadec fields. There are differences in the evolutionary trends for individual dacite-matrix pairs in this variation diagram. Thus, Balmoral and Fonualei trends increase in  $\text{Al}_2\text{O}_3/\text{TiO}_2$ , while Metis Shoal and Herald Cays trends decrease in  $\text{Al}_2\text{O}_3/\text{TiO}_2$ , suggesting a similar evolution for Balmoral and Fonualei dacites.

The main Balmoral pumice glass (P2) is notable for its extremely depleted incompatible element pattern. The values (ppm) for Nd (3.5), Sr (21), Ba (33) and Zr (18) are comparable to those in Mid-Ocean Ridge Basalts (Ewart & Hawkesworth, 1987), where average depleted and normal MORB values show Nd (2–8), Sr (40–140), Ba

(1–20) and Zr (14–90). Considerable variations in incompatible element values exist between this depleted Balmoral pumice and other Balmoral pumices (see Table 4 and Fig. 10). Excluding the unusual pumice (P7), Balmoral pumices range in Nd (3–7), Sr (21–388), Ba (33–643) and Zr (18–50). Such variable enrichments are a feature of the Tonga-Kermadec arc (Ewart & Hawkesworth, 1987; Ewart *et al.*, 1998), where the greatest HFS-element depletions appear at the north end. This would favour a northern Tonga source for most Balmoral pumices.

Over the past 150 years, the only recorded source of olivine-bearing low K-dacite in the Southwest Pacific region is at Metis Shoal (Melson *et al.*, 1970). However, activity here may not have produced the main Balmoral

pumice, as incompatible trace elements for the 1967–1968 eruption dacite are far more enriched (Ewart *et al.*, 1973; Kay & Hubbard, 1978) compared to the depleted Balmoral glass (Table 4). A Metis Shoal source therefore would need considerable source enrichment over a 3300 year evolution. The later olivine-dacite (P4) is closer to Metis Shoal dacite in its trace element pattern. A more northern HFS-depleted Tonga source is proposed for the main pumice, particularly as submarine pumice rafts also emanate from the extreme north of the Tongan arc (Curaçoa Reef; Latter, 1976). The Ba/Th ratio (330) and low Nd (3.5 ppm) for the main Balmoral dacite (P2) are compatible with values for the northern Tafahi-Niuatoputapu island group, while higher Ba/Th (792–1608) and Nd (4–7.1 ppm) values for other Balmoral dacites (P4, P6) are more compatible with Tongan island sources lying south of this group (Turner & Hawkesworth, 1997).

**Alternative sources.** Oceanic current flows off eastern Australia may have varied over the last 2000–3000 years, so sources other than Tonga are possible, e.g., Kermadec sources. However, on present current flow directions, pumice from Kermadec sources would encounter prevailing east to west current flows related to the return flow of the East Australian Current. Other possibilities include sources around the Fiji, Vanuatu and Norfolk Basins, where pumice sightings and strandings are also recorded (Bryan, 1968; W.R. Dickinson, pers. comm. 1997). However, pumice (W.R. Dickinson sample) from a palaeostranding at Sigatoka, Fiji, of similar age range to the Balmoral strandings appears petrologically distinct to the Balmoral material. Low-K silicic rocks are found in a few Vanuatu centres (Carney *et al.*, 1985; Peate *et al.*, 1997), but are relatively lower in silica (< 64 wt% SiO<sub>2</sub>) than the Balmoral, Herald Cays and Tongan dacites. Pumice sources further north in the Solomon, Bouganville and New Britain island arcs also need consideration. Drifts from these sources, however, would meet northward flowing circulation of the Hiri Current, the northerly extension of the Southern Equatorial Current (Burrage, 1993) and so would be impeded in reaching New South Wales coasts.

The main Balmoral palaeopumice layer shows concentrated packing of pumice within a relatively uniform sandy matrix (Attenbrow & Hashimoto, in prep.), favouring its accumulation by onshore westerly drift through the oceanic entrance to Port Jackson. Such deposition would precede growth of high dunes on the developing sand barrier. Although it could be driven in by offshore storm activity, the pumice deposit differs from the highly mixed fine and coarse pumice-bearing deposits attributed to episodic tsunamic scouring along the New South Wales coast (Bryant *et al.*, 1992a, 1992b). However, sparse pumice (P4) mixed in later 1800–2800 myr deposits at Balmoral conceivably may be transported by large waves overtopping a higher dune barrier.

Pumice glasses analysed from the main Balmoral layer show some distinct trace element differences between samples recovered from inside the rock shelter (P2) and from outside (P1) the shelter. This could suggest that

pumices related to separate eruptions are present in this stratigraphic interval, even though all show a similar olivine-bearing porphyritic dacite character. The dates for these two pumice exposures (3280 ± 60 myrs and 3250 ± 90 myrs) are indistinguishable within error, so this cannot be resolved at this stage. In any event, this pumice layer is intercalated within an aboriginal occupation site which suggests that these peak pumice strandings were witnessed by local inhabitants. Although the precise external source that erupted the main Balmoral pumice influx requires further confirmation, the suggested northern Tonga source would imply a drift of some 4000 km.

**ACKNOWLEDGMENTS.** R. Pogson, S. Folwell and R. Springthorpe (Australian Museum) assisted with preparation of the script. N. Pearson (Macquarie University) provided facilities for EMP and laser ablation ICP-MS analyses. V. Attenbrow (Australian Museum) and R. Hashimoto (University of Sydney) assisted with interpretations of the Balmoral Beach archaeological site and W.R. Dickinson (University of Arizona) assisted with information on Fiji pumice strandings. P.C. Rickwood (University of New South Wales) reviewed the script. The project was supported by a grant from the Australian Museum to the Geodiversity Research Centre.

## References

- Attenbrow, V., F.L. Sutherland, B.J. Barron & R. Hashimoto, 1997. Balmoral Beach Aboriginal Shell Midden—Origin and Chronology of Pumice. Sixth Australasian Archaeometry Abstracts, Feb 10–13, AINSE, ANSTO, Australian Museum, Sydney.
- Bryan, W.B., 1968. Low-potash dacite drift pumice from the Coral Sea. *Geological Magazine* 105: 431–439.
- Bryan, W.B., 1979. Low-K<sub>2</sub>O dacite from the Tongan-Kermadec Island Arc: petrography, chemistry, petrogenesis. In: *Trondhjemites, Dacites and Related Rocks*, ed. F. Barker, pp. 581–600. New York: Elsevier.
- Bryan, W.B., G.D. Stice & A. Ewart, 1972. Geology, petrography and geochemistry of the volcanic islands of Tonga. *Journal of Geophysical Research* 77: 1566–1585.
- Bryant, E.A., R.W. Young, D.M. Price & S.A. Short, 1992a. Evidence for Pleistocene and Holocene raised marine deposits, Sandon Point, New South Wales. *Australian Journal of Earth Sciences* 39: 481–493.
- Bryant, E.A., R.W. Young & D.M. Price, 1992b. Evidence for tsunami sedimentation on the southeastern coast of Australia. *The Journal of Geology* 100: 753–765.
- Burrage, D.M., 1993. Coral Sea currents, the seas around us—number 3. *Corella* 17: 135–145.
- Carney, J.N., A. Macfarlane & D.I.J. Mallick, 1985. The Vanuatu Island Arc: an outline of the stratigraphy, structure, and petrology. In *The Ocean Basins and Margins Vol. 7A. The Pacific Ocean*, eds. A.E.M. Nair, F.G. Stehli and S. Uyeda, pp. 683–718. New York: Plenum Press.
- Clarke, W.B., 1842. On the occurrence of atmospheric deposits of dust and ashes, with remarks on the drift pumice of the coasts of New Holland. *Tasmanian Journal of Natural Science*, Hobart I(V): 321–341.
- Clift, P.D., & P.Z. Vroon, 1996. Isotopic evolution of the Tonga Arc during Lau Basin rifting; evidence from the volcanoclastic record. *Journal of Petrology* 37: 1153–1173.

- Coombs, D.S., & C.A. Landis, 1966. Pumice from the South Sandwich Eruption of March 1962 reaches New Zealand. *Nature* 209: 289–290.
- Droop, G.T.R., 1987. A general equation for estimating Fe<sup>3+</sup> concentrations in ferromagnesian silicates and oxides from microprobe analyses, using stoichiometric criteria. *Mineralogical Magazine* 51: 431–435.
- Ewart, A., R.N. Brothers & A. Mateen, 1977. An outline of the geology and geochemistry, and the possible petrogenetic evolution of the volcanic rocks of the Tonga-Kermadec-New Zealand island arc. *Journal of Volcanology and Geothermal Research* 2: 205–250.
- Ewart, A., & W.B. Bryan, 1973. The petrology and geochemistry of the Tongan Island. In *The Western Pacific: Island Arcs, Marginal Seas, Geochemistry*, ed. P.J. Coleman, pp. 503–522. Perth: University of Western Australian Press.
- Ewart, A., W.B. Bryan & J.B. Gill, 1973. Mineralogy and geochemistry of the younger volcanic islands of Tonga, S.W. Pacific. *Journal of Petrology* 14: 429–465.
- Ewart, A., K.D. Collerson, M. Regelous, J.I. Wendt & Y. Niu, 1998. Geochemical evolution within the Tonga-Kermadec-Lau Arc-Back-arc systems: the role of varying mantle wedge composition in space and time. *Journal of Petrology* 39(3): 331–368.
- Ewart, A., & C.J. Hawkesworth, 1987. The Pleistocene-Recent Tonga-Kermadec Arc Lavas: interpretation of new isotopic and rare earth data in terms of a depleted mantle source model. *Journal of Petrology* 28: 495–528.
- Frick, C., & L.E. Kent, 1984. Drift pumice in the Indian and South Atlantic Oceans (volcanic eruptions). *Transactions Geological Society of South Africa* 87: 19–33.
- Hughes, C.J., 1982. *Igneous Petrology. Development in Petrology* 7. Amsterdam: Elsevier.
- Jokiel, P.L., 1990. Transport of reef corals into the Great Barrier Reef. *Nature* 347: 665–667.
- Kay, R.W., & N.J. Hubbard, 1978. Trace elements in ocean ridge basalts. *Earth and Planetary Science Letters* 38: 95–116.
- Latter, J.H., 1976. Variations in stress release preceding and accompanying a submarine eruption in northern Tonga. In *Volcanism in Australasia*, ed. R.W. Johnson, pp. 355–373. Amsterdam: Elsevier.
- Little, I.P., & W.T. Ward, 1980. Use of chemical data for classification of pumices from sandy beach deposits in southeastern Queensland. CSIRO Division of Soils, Divisional Report 48, pp. 14.
- Lloyd, E.F., & S. Nathan, 1981. Geology and tephrochronology of Raoul Island, Kermadec Group, New Zealand. *Bulletin Geological Survey of New Zealand* 95: 1–105.
- Loucks, R.R., 1996. A precise olivine-augite Mg-Fe-exchange geothermometer. *Contributions to Mineralogy and Petrology* 125: 140–150.
- Martinez, J.I., 1994. Late Pleistocene carbonate dissolution patterns in the Tasman Sea. In *Evolution of the Tasman Sea Basin*, eds. G.J. van der Lingen, K.M. Swanson & R.J. Muir, pp. 215–228. Rotterdam: A.A. Balkema.
- Melson, W.G., E. Jarosewich & C.A. Lundquist, 1970. Volcanic eruption at Metis Shoal, Tonga, 1967–1968: description and petrology. *Smithsonian Contributions to Earth Sciences* 4: 1–18.
- Nelson, C.S., C.H. Hendy & A.M. Cuthbertson, 1994. Oxygen isotope evidence for climatic contrasts between Tasman Sea and Southwest Pacific Ocean during the late Quaternary. In *Evolution of the Tasman Sea Basin*, eds. G.J. Van der Lingen, K.M. Swanson & R.J. Muir, pp. 181–196. Rotterdam: A.A. Balkema.
- Norman, M.D., N.J. Pearson, A. Sharma & W.L. Griffin, 1996. Quantitative analysis of trace elements in geological materials by laser ablation ICPMS: Instrumental operating conditions and calibration values of NIST glasses. *Geostandards Newsletter* 20(2): 247–261.
- Peate, D.W., J.A. Pearce, C.J. Hawkesworth, H. Colley, C.M.H. Edwards & K. Hirose, 1997. Geochemical variations in Vanuatu arc lavas: the role of subducted material and a variable mantle wedge composition. *Journal of Petrology* 38: 1331–1358.
- Pullar, W.A., B.P. Kohn & J.E. Cox, 1977. Air-fall Kaharoa Ash and Taupo Pumice and sea-rafted Loiseles Pumice, Taupo Pumice, and Leigh Pumice in northern and eastern parts of the North Island, New Zealand. *New Zealand Journal of Geology and Geophysics* 20: 697–717.
- Reed, S.J.B., 1975. *Electron Microprobe Analysis*. Cambridge: Cambridge University Press.
- Rotschi, H., & L. Le Masson, 1967. Oceanography of the Coral and Tasman Seas. *Oceanography and Marine Biology Annual Review* 5: 49–97.
- Stanton, J.B., 1992. Proposed south-western Pacific sources for drift pumice collected from the north Queensland coast between Cardwell and Cape Upstart. Unpublished B.Sc(Hons) thesis. Townsville: James Cook University of North Queensland.
- Sutherland, F.L., 1965. Dispersal of pumice, supposedly from the 1962 South Sandwich Islands eruption, on southern Australian shores. *Nature* 207: 1332–1335.
- Sutherland, F.L., & A.M. Olsen, 1968. The persistence of drift pumice from the 1962 South Sandwich Islands eruption, in Southern Australian waters. *Papers and Proceedings of the Royal Society of Tasmania* 102: 1–5.
- Taylor, S.R., & S.M. McLennan, 1985. *The Continental Crust: Its Compositions and Evolution*. Oxford: Blackwell Scientific Publications.
- Tomczak, M., & D. Hao, 1989. Water masses in the thermocline of the Coral Sea. *Deep-Sea Research* 36: 1503–1514.
- Turner, S., & C. Hawkesworth, 1997. Constraints on flux rates and mantle dynamics beneath island arcs from Tonga-Kermadec lava geochemistry. *Nature* 389: 568–573.
- Wells, P.R.A., 1977. Pyroxene thermometry in simple and complex systems. *Contributions to Mineralogy and Petrology* 62: 129–139.
- Wilson, M., 1989. *Igneous Petrogenesis: A Global Tectonic Approach*. London: Unwin Hyman.
- Wood, B.J., & S. Banno, 1973. Garnet orthopyroxene and orthopyroxene-clinopyroxene relations in simple and complex systems. *Contributions to Mineralogy and Petrology* 42: 109–121.

Manuscript received 19 August 1997, revised 30 December 1997 and accepted 1 April 1998.

Assoc. Eds.: V.J. Attenbrow & J.R. Specht.

**Table 1.** Summary of characteristics of pumice from the Balmoral Beach site.

| stratigraphic level (age B.P.)         | sample numbers | crystals volume | mineral proportions (approx. % by volume)          | glass type (%SiO <sub>2</sub> ) | vesicles % voids |
|--|----------------|-----------------|--|---------------------------------|------------------|
| <b>later levels</b><br>1800–2800 yrs   | P4             | 3%              | Pl(50%),Opx(30%),Cpx(20%)<br>Ol,Ox                 | rhyodacite<br>(73–74%)          | > 60 – < 80%     |
| <b>main level</b><br>3300 yrs          | P1             | 5%              | Pl(50%),Cpx(20%),Opx(15%)<br>Ox(10%),Ol(<5%)       | rhyodacite<br>(72–73%)          | > 60 – < 80%     |
|  | P2             | 3–4%            | Pl(50%),Opx(30%),Cpx(10%)<br>Ol(<5%),Ox(<5%),Ap    | rhyodacite<br>(73%)             | > 60 – < 80%     |
|  | P5             | 5%              | Pl(55%),Opx(20%),Cpx(20%)<br>Ox(<3%),Ol(<2%),Ap,Zr | rhyodacite<br>(74–75%)          | > 60 – < 80%     |
| <b>earlier levels</b><br>3300–3500 yrs | P3             | 2%              | Opx(50%),Cpx(40%),Pl(10%)<br>Ox                    | rhyodacite                      | > 60 – < 80%     |
|  | P6             | 3%              | Pl(50%),Opx(30%),Cpx(10%)<br>Ox(10%)               | rhyodacite<br>(75–76%)          | > 60 – < 80%     |
|  | P7             | 1%              | Qz, Opx, Cpx?, Pl, Ox                              | rhyodacite<br>(77%)             | > 60 – < 80%     |

Pl, plagioclase feldspar; Opx, orthopyroxene; Cpx, clinopyroxene; Ox, iron oxide; Ol, olivine; Qz, quartz; Ap, apatite; Zr, zircon.

**Table 2.** Representative analyses, pumice xenocrysts/phenocrysts, Balmoral Beach site.**2A pumice P1 (3,200–3,300 years)**

| mineral<br>wt%                 | Ol<br>(1) | Ol<br>(2) | Cpx<br>(c) | Cpx<br>(r) | Opx   | Pl<br>(1) | Pl<br>(2) | FeOx<br>(1)         | FeOx<br>(2)        |
|--------------------------------|-----------|-----------|------------|------------|-------|-----------|-----------|---------------------|--------------------|
| SiO <sub>2</sub>               | 40.65     | 38.71     | 52.88      | 52.30      | 51.34 | 50.26     | 56.34     | 0.09                | 0.01               |
| TiO <sub>2</sub>               | 0.01      | 0.05      | 0.16       | 0.21       | 0.17  | 0.00      | 0.04      | 0.00                | 47.62              |
| Al <sub>2</sub> O <sub>3</sub> | 0.03      | 0.03      | 2.28       | 3.03       | 0.69  | 30.60     | 26.38     | 0.01                | 0.19               |
| Cr <sub>2</sub> O <sub>3</sub> | 0.05      | 0.01      | 0.14       | 0.14       | 0.00  | 0.00      | 0.00      | 0.01                | 0.00               |
| MgO                            | 49.36     | 42.85     | 17.11      | 16.53      | 18.43 | 0.00      | 0.00      | 0.00                | 2.05               |
| CaO                            | 0.27      | 0.23      | 23.30      | 23.08      | 1.54  | 14.26     | 9.80      | 0.10                | 0.01               |
| MnO                            | 0.10      | 0.36      | 0.15       | 0.08       | 1.40  | 0.00      | 0.01      | 0.19                | 1.06               |
| FeO                            | 9.63      | 17.32     | 3.74       | 4.46       | 25.59 | 0.40      | 0.38      | 80.82               | 47.69              |
| NiO                            | 0.21      | 0.10      | 0.06       | 0.00       | 0.00  | 0.06      | 0.02      | 0.09                | 0.09               |
| Na <sub>2</sub> O              | 0.03      | 0.00      | 0.11       | 0.14       | 0.01  | 3.37      | 6.01      | 0.00                | 0.01               |
| K <sub>2</sub> O               | 0.00      | 0.00      | 0.00       | 0.01       | 0.00  | 0.01      | 0.07      | 0.00                | 0.00               |
| total                          | 100.34    | 99.66     | 99.93      | 99.98      | 99.17 | 98.96     | 99.05     | 81.31               | 98.73              |
| cations                        | 4[O]      | 4[O]      | 6[O]       | 6[O]       | 6[O]  | 32[O]     | 32[O]     | 32[O]               | 6[O]               |
| Si <sup>4+</sup>               | 0.994     | 0.989     | 1.935      | 1.916      | 1.975 | 9.267     | 10.238    | 0.032               | 0.000              |
| Ti <sup>4+</sup>               | 0.000     | 0.001     | 0.004      | 0.006      | 0.005 | 0.000     | 0.006     | 0.000               | 1.791              |
| Al <sup>3+</sup>               | 0.001     | 0.001     | 0.098      | 0.131      | 0.031 | 6.650     | 5.650     | 0.004               | 0.011              |
| Cr <sup>3+</sup>               | 0.001     | 0.000     | 0.004      | 0.004      | 0.000 | 0.000     | 0.000     | 0.003               | 0.000              |
| Mg <sup>2+</sup>               | 1.799     | 1.632     | 0.933      | 0.903      | 1.058 | 0.000     | 0.000     | 0.000               | 0.153              |
| Ca <sup>2+</sup>               | 0.007     | 0.006     | 0.910      | 0.906      | 0.064 | 2.817     | 1.908     | 0.038               | 0.000              |
| Mn <sup>2+</sup>               | 0.002     | 0.008     | 0.005      | 0.003      | 0.046 | 0.000     | 0.002     | 0.057               | 0.045              |
| Fe <sup>2+</sup>               | 0.197     | 0.370     | 0.114      | 0.137      | 0.824 | 0.062     | 0.058     | 7.912               | 1.588              |
| Fe <sup>3+</sup>               | 0.000     | 0.000     | 0.000      | 0.000      | 0.000 | 0.000     | 0.000     | 15.929              | 0.407              |
| Ni <sup>2+</sup>               | 0.004     | 0.002     | 0.002      | 0.000      | 0.000 | 0.009     | 0.003     | 0.025               | 0.004              |
| Na <sup>1+</sup>               | 0.001     | 0.000     | 0.008      | 0.010      | 0.001 | 1.205     | 2.118     | 0.000               | 0.001              |
| K <sup>1+</sup>                | 0.000     | 0.000     | 0.000      | 0.001      | 0.000 | 0.002     | 0.016     | 0.000               | 0.000              |
| sum                            | 3.006     | 3.009     | 4.013      | 4.017      | 4.004 | 20.012    | 19.999    | 24.000 <sup>1</sup> | 4.000 <sup>1</sup> |

Ol(1), olivine(?) xenocryst; Ol(2), olivine phenocryst; Cpx(c), core of zoned phenocryst; Cpx(r), rim of zoned phenocryst; Opx, orthopyroxene phenocryst; Pl(1), plagioclase glomerophenocryst; Pl(2), zoned plagioclase xenocryst; FeOx(1), intersertal iron oxide in plagioclase glomerophenocryst Pl(1); FeOx(2), small euhedral grain.

<sup>1</sup> Fe<sup>2+</sup> and Fe<sup>3+</sup> recalculated from total FeO after the method of Droop (1987) and assigned on ideal stoichiometry.

**Table 2 (cont.).** Representative analyses, pumice xenocrysts/phenocrysts, Balmoral Beach site.**2B pumice P2 (3,200–3,300 years)**

| mineral<br>wt%                 | Ol      | Cpx<br>(1) | Cpx<br>(2) | Opx<br>(1) | Opx<br>(2) | Pl<br>(c) | Pl<br>(r) | FeOx                | FeOx<br>(1)         |
|--------------------------------|---------|------------|------------|------------|------------|-----------|-----------|---------------------|---------------------|
| SiO <sub>2</sub>               | 41.25   | 52.40      | 51.02      | 50.51      | 51.54      | 51.51     | 53.49     | 0.12                | 0.02                |
| TiO <sub>2</sub>               | 0.00    | 0.13       | 0.25       | 0.28       | 0.18       | 0.02      | 0.01      | 14.42               | 0.83                |
| Al <sub>2</sub> O <sub>3</sub> | 0.04    | 2.57       | 0.96       | 0.82       | 0.52       | 30.00     | 28.75     | 2.13                | 0.00                |
| Cr <sub>2</sub> O <sub>3</sub> | 0.00    | 0.35       | 0.00       | 0.03       | 0.03       | 0.00      | 0.00      | 0.00                | 0.00                |
| MgO                            | 42.36   | 16.99      | 11.74      | 17.26      | 18.70      | 0.00      | 0.00      | 1.27                | 0.00                |
| CaO                            | 0.22    | 23.09      | 19.05      | 1.64       | 1.54       | 13.62     | 12.16     | 0.01                | 0.01                |
| MnO                            | 0.25    | 0.04       | 0.91       | 1.48       | 1.38       | 0.00      | 0.04      | 0.81                | 0.08                |
| FeO                            | 15.75   | 3.85       | 15.31      | 27.09      | 25.48      | 0.45      | 0.63      | 75.89               | 79.89               |
| NiO                            | 0.09    | 0.02       | 0.00       | 0.00       | 0.08       | 0.01      | 0.04      | 0.01                | 0.00                |
| Na <sub>2</sub> O              | 0.00    | 0.11       | 0.22       | 0.02       | 0.02       | 3.98      | 4.63      | 0.00                | 0.00                |
| K <sub>2</sub> O               | 0.04    | 0.00       | 0.00       | 0.00       | 0.00       | 0.02      | 0.04      | 0.03                | 0.00                |
| total                          | 100.00* | 99.55      | 99.46      | 99.13      | 99.47      | 99.61     | 99.79     | 94.69               | 80.83               |
| cations                        | 4[O]    | 6[O]       | 6[O]       | 6[O]       | 6[O]       | 32[O]     | 32[O]     | 32[O]               | 32[O]               |
| Si <sup>4+</sup>               | 1.035   | 1.924      | 1.965      | 1.964      | 1.977      | 9.423     | 9.728     | 0.007               | 0.036               |
| Ti <sup>4+</sup>               | 0.000   | 0.004      | 0.007      | 0.008      | 0.005      | 0.003     | 0.001     | 0.222               | 3.271               |
| Al <sup>3+</sup>               | 0.001   | 0.111      | 0.044      | 0.038      | 0.024      | 6.468     | 6.162     | 0.000               | 0.757               |
| Cr <sup>3+</sup>               | 0.000   | 0.010      | 0.000      | 0.001      | 0.001      | 0.000     | 0.000     | 0.000               | 0.000               |
| Mg <sup>2+</sup>               | 1.584   | 0.930      | 0.674      | 1.000      | 1.070      | 0.000     | 0.000     | 0.000               | 0.571               |
| Ca <sup>2+</sup>               | 0.006   | 0.908      | 0.786      | 0.068      | 0.063      | 2.669     | 2.369     | 0.004               | 0.003               |
| Mn <sup>2+</sup>               | 0.005   | 0.001      | 0.030      | 0.049      | 0.045      | 0.000     | 0.006     | 0.024               | 0.207               |
| Fe <sup>2+</sup>               | 0.331   | 0.118      | 0.493      | 0.881      | 0.818      | 0.069     | 0.096     | 8.201               | 10.500              |
| Fe <sup>3+</sup>               | 0.000   | 0.000      | 0.000      | 0.000      | 0.000      | 0.000     | 0.000     | 15.542              | 8.641               |
| Ni <sup>2+</sup>               | 0.002   | 0.001      | 0.000      | 0.000      | 0.003      | 0.002     | 0.006     | 0.000               | 0.002               |
| Na <sup>1+</sup>               | 0.000   | 0.008      | 0.016      | 0.002      | 0.002      | 1.412     | 1.633     | 0.000               | 0.000               |
| K <sup>1+</sup>                | 0.001   | 0.000      | 0.000      | 0.000      | 0.000      | 0.005     | 0.009     | 0.000               | 0.012               |
| sum                            | 2.965   | 4.015      | 4.015      | 4.011      | 4.008      | 20.051    | 20.010    | 24.000 <sup>1</sup> | 24.000 <sup>1</sup> |

Ol, olivine phenocryst; Cpx(1), resorbed clinopyroxene; Cpx(2), clinopyroxene phenocryst in glomeroporphyritic Cpx, Opx, Pl, FeOx cluster; Opx(1), orthopyroxene phenocryst; Opx(2), orthopyroxene phenocryst with Cpx intergrowth; Pl(c), core of zoned plagioclase phenocryst in glomeroporphyritic Cpx, Opx, Pl, FeOx cluster with Cpx(2); Pl(r), rim of zoned plagioclase Pl(c); FeOx, iron-titanium oxide intergrowth with plagioclase glomerophenocrysts; FeOx(1), iron oxide in iron-titanium oxide FeO(x).

<sup>1</sup> Fe<sup>2+</sup> and Fe<sup>3+</sup> recalculated from total FeO after the method of Droop (1987) and assigned on ideal stoichiometry.

\* normalised analysis.

**Table 2 (cont.).** Representative analyses, pumice xenocrysts/phenocrysts, Balmoral Beach site.**2C pumice P4 (>1,800–<2,800 years), pumice P5 (3,200–3,300 years)**

| mineral<br>wt%                 | Ol<br>(P4) | Cpx<br>(P4) | Opx<br>(P4) | Pl<br>(P4) | FeOx<br>(P4)        | Cpx<br>(P5) | Opx<br>(P5) | Pl<br>(P5)          | FeOx<br>(P5)        |
|--------------------------------|------------|-------------|-------------|------------|---------------------|-------------|-------------|---------------------|---------------------|
| SiO <sub>2</sub>               | 40.68      | 51.08       | 51.84       | 52.29      | 0.10                | 52.52       | 51.10       | 51.34               | 0.14                |
| TiO <sub>2</sub>               | 0.00       | 0.28        | 0.26        | 0.04       | 10.05               | 0.22        | 0.20        | 0.02                | 14.54               |
| Al <sub>2</sub> O <sub>3</sub> | 0.00       | 1.33        | 1.06        | 29.02      | 2.24                | 2.60        | 0.61        | 29.93               | 2.11                |
| Cr <sub>2</sub> O <sub>3</sub> | 0.05       | 0.00        | 0.00        | 0.00       | 0.07                | 0.20        | 0.00        | 0.00                | 0.00                |
| MgO                            | 48.75      | 12.80       | 20.71       | 0.00       | 1.29                | 16.97       | 17.99       | 0.00                | 1.18                |
| CaO                            | 0.28       | 19.36       | 1.48        | 12.65      | 0.08                | 23.49       | 1.51        | 13.75               | 0.00                |
| MnO                            | 0.17       | 0.57        | 1.27        | 0.00       | 0.39                | 0.09        | 1.55        | 0.00                | 0.92                |
| FeO                            | 10.71      | 14.31       | 23.35       | 0.43       | 80.29               | 3.98        | 26.67       | 0.64                | 77.68               |
| NiO                            | 0.16       | 0.04        | 0.00        | 0.00       | 0.08                | 0.13        | 0.01        | 0.00                | 0.00                |
| Na <sub>2</sub> O              | 0.00       | 0.15        | 0.00        | 4.39       | 0.00                | 0.17        | 0.04        | 3.73                | 0.00                |
| K <sub>2</sub> O               | 0.00       | 0.00        | 0.00        | 0.03       | 0.00                | 0.00        | 0.00        | 0.03                | 0.01                |
| total                          | 100.80     | 99.92       | 99.97       | 98.85      | 94.59               | 100.27      | 99.68       | 99.44               | 96.58               |
| cations                        | 4[O]       | 6[O]        | 6[O]        | 32[O]      | 32[O]               | 6[O]        | 6[O]        | 32[O]               | 32[O]               |
| Si <sup>4+</sup>               | 0.995      | 1.947       | 1.957       | 9.606      | 0.030               | 1.917       | 1.969       | 9.413               | 0.041               |
| Ti <sup>4+</sup>               | 0.000      | 0.008       | 0.007       | 0.006      | 2.270               | 0.006       | 0.006       | 0.003               | 3.237               |
| Al <sup>3+</sup>               | 0.000      | 0.060       | 0.047       | 6.289      | 0.793               | 0.112       | 0.028       | 6.468               | 0.736               |
| Cr <sup>3+</sup>               | 0.000      | 0.000       | 0.000       | 0.000      | 0.017               | 0.006       | 0.000       | 0.000               | 0.000               |
| Mg <sup>2+</sup>               | 1.777      | 0.728       | 1.166       | 0.000      | 0.578               | 0.924       | 1.034       | 0.000               | 0.521               |
| Ca <sup>2+</sup>               | 0.007      | 0.791       | 0.060       | 2.492      | 0.026               | 0.919       | 0.062       | 2.701               | 0.000               |
| Mn <sup>2+</sup>               | 0.004      | 0.018       | 0.041       | 0.000      | 0.099               | 0.003       | 0.051       | 0.000               | 0.231               |
| Fe <sup>2+</sup>               | 0.220      | 0.456       | 0.734       | 0.066      | 9.578               | 0.122       | 0.860       | 0.098               | 10.519              |
| Fe <sup>3+</sup>               | 0.000      | 0.000       | 0.000       | 0.000      | 10.590              | 0.000       | 0.000       | 0.000               | 8.711               |
| Ni <sup>2+</sup>               | 0.003      | 0.001       | 0.000       | 0.000      | 0.019               | 0.004       | 0.000       | 0.000               | 0.000               |
| Na <sup>1+</sup>               | 0.000      | 0.011       | 0.000       | 1.565      | 0.000               | 0.012       | 0.003       | 1.326               | 0.000               |
| K <sup>1+</sup>                | 0.000      | 0.000       | 0.000       | 0.007      | 0.000               | 0.000       | 0.000       | 0.007               | 0.004               |
| sum                            | 3.006      | 4.020       | 4.012       | 20.031     | 24.000 <sup>1</sup> | 4.025       | 4.013       | 20.016 <sup>1</sup> | 24.000 <sup>1</sup> |

Ol(P4), olivine phenocryst (part resorbed); Cpx(P4), clinopyroxene phenocryst in Cpx, Opx, Pl, FeOx glomeroporphyritic cluster; Opx(P4), orthopyroxene phenocrysts in Cpx, Opx, Pl, FeOx glomeroporphyritic cluster; Cpx(P5), clinopyroxene phenocryst intergrowth with Ol; Opx(P5), orthopyroxene phenocryst containing apatite, opaque oxides and glass inclusions; Pl(P5), zoned plagioclase phenocryst in Opx, Pl, FeOx and amphibole(?) glomeroporphyritic cluster.

<sup>1</sup> Fe<sup>2+</sup> and Fe<sup>3+</sup> recalculated from Total FeO after the method of Droop (1987) and assigned on ideal stoichiometry.

**Table 2 (cont.).** Representative analyses, pumice xenocrysts/phenocrysts, Balmoral Beach site.**2D pumice P6 (c. 3300 years), pumice P7 (c. 3,500 years)**

| mineral<br>wt%                 | Cpx<br>(P6) | Opx<br>(P6) | Pl<br>(P6) | FeOx<br>(P6)        | FeS<br>(P6) | Cpx<br>(P7) | Opx<br>(P7) | Pl<br>(P7) | FeOx<br>(P7)        |
|--------------------------------|-------------|-------------|------------|---------------------|-------------|-------------|-------------|------------|---------------------|
| SiO <sub>2</sub>               | 51.26       | 52.33       | 46.94      | 0.06                | 0.03        | 51.15       | 52.20       | 51.07      | 0.06                |
| TiO <sub>2</sub>               | 0.28        | 0.17        | 0.00       | 11.10               | 0.00        | 0.33        | 0.06        | 0.18       | 10.79               |
| Al <sub>2</sub> O <sub>3</sub> | 1.44        | 0.94        | 32.81      | 2.06                | 0.01        | 1.33        | 29.03       | 0.60       | 2.06                |
| Cr <sub>2</sub> O <sub>3</sub> | 0.00        | 0.01        | 0.04       | 0.05                | 0.00        | 0.00        | 0.05        | 0.00       | 0.00                |
| MgO                            | 12.90       | 21.21       | 0.00       | 1.09                | 0.00        | 13.04       | 0.00        | 17.32      | 1.06                |
| CaO                            | 20.23       | 1.59        | 17.30      | 0.03                | 0.37        | 19.60       | 13.12       | 1.66       | 0.03                |
| MnO                            | 0.57        | 0.89        | 0.03       | 0.49                | 0.04        | 0.60        | 0.03        | 1.00       | 0.55                |
| FeO                            | 13.05       | 22.94       | 0.84       | 81.20               | 79.10       | 13.70       | 0.57        | 27.40      | 79.71               |
| NiO                            | 0.00        | 0.00        | 0.03       | 0.09                | 0.10        | 0.00        | 0.09        | 0.01       | 0.04                |
| Na <sub>2</sub> O              | 0.18        | 0.03        | 1.84       | 0.00                | 0.00        | 0.16        | 4.06        | 0.03       | 0.00                |
| K <sub>2</sub> O               | 0.02        | 0.00        | 0.00       | 0.03                | 0.00        | 0.00        | 0.05        | 0.00       | 0.01                |
| total                          | 99.94       | 100.11      | 99.97      | 96.17               | 79.57       | 99.91       | 99.36       | 99.27      | 94.31               |
| cations                        | 6[O]        | 6[O]        | 32[O]      | 32[O]               |             | 6[O]        | 6[O]        | 32[O]      | 32[O]               |
| Si <sup>4+</sup>               | 1.947       | 1.964       | 8.682      | 0.018               |             | 1.946       | 1.979       | 9.559      | 0.018               |
| Ti <sup>4+</sup>               | 0.008       | 0.005       | 0.000      | 2.475               |             | 0.009       | 0.005       | 0.008      | 2.453               |
| Al <sup>3+</sup>               | 0.065       | 0.042       | 7.153      | 0.720               |             | 0.060       | 0.027       | 6.272      | 0.734               |
| Cr <sup>3+</sup>               | 0.000       | 0.000       | 0.006      | 0.012               |             | 0.000       | 0.000       | 0.007      | 0.000               |
| Mg <sup>2+</sup>               | 0.730       | 1.187       | 0.000      | 0.482               |             | 0.740       | 1.000       | 0.000      | 0.478               |
| Ca <sup>2+</sup>               | 0.823       | 0.064       | 3.429      | 0.010               |             | 0.799       | 0.069       | 2.577      | 0.010               |
| Mn <sup>2+</sup>               | 0.018       | 0.028       | 0.005      | 0.123               |             | 0.019       | 0.033       | 0.005      | 0.141               |
| Fe <sup>2+</sup>               | 0.415       | 0.720       | 0.130      | 9.857               |             | 0.436       | 0.888       | 0.087      | 9.825               |
| Fe <sup>3+</sup>               | 0.000       | 0.000       | 0.000      | 10.282              |             | 0.000       | 0.000       | 0.000      | 10.327              |
| Ni <sup>2+</sup>               | 0.000       | 0.000       | 0.005      | 0.021               |             | 0.012       | 0.000       | 0.013      | 0.010               |
| Na <sup>1+</sup>               | 0.013       | 0.002       | 0.660      | 0.000               |             | 0.000       | 0.002       | 1.479      | 0.000               |
| K <sup>1+</sup>                | 0.001       | 0.000       | 0.000      | 0.000               |             | 0.000       | 0.000       | 0.012      | 0.004               |
| sum                            | 4.020       | 4.012       | 20.070     | 24.000 <sup>1</sup> |             | 4.021       | 4.003       | 20.029     | 24.000 <sup>1</sup> |

Cpx(P6), clinopyroxene phenocryst with plagioclase inclusions; Opx(P6), orthopyroxene phenocryst with intergrown plagioclase and FeOx; Pl(P6), plagioclase intergrowth with orthopyroxene Opx(P6); FeS, iron sulphide inclusions in Cpx, Opx, Pl glomeroporphyritic cluster; Cpx(P7), clinopyroxene phenocryst; Opx(P7), orthopyroxene phenocryst; Pl(P7), plagioclase phenocryst; FeOx(P7), iron oxide phenocryst intergrowth with Cpx.

<sup>1</sup> Fe<sup>2+</sup> and Fe<sup>3+</sup> recalculated from total FeO after the method of Droop (1987) and assigned on ideal stoichiometry.

**Table 3.** Representative analyses of glass from pumice samples, Balmoral Beach site.

| wt%   | P1    | P2    | P2(i) | P4    | P5    | P5(i) | P6    | P7    | P7(i) |
|---|-------|-------|-------|-------|-------|-------|-------|-------|-------|
| SiO <sub>2</sub>  | 72.22 | 72.98 | 68.94 | 73.47 | 74.13 | 71.40 | 75.31 | 76.98 | 72.51 |
| TiO <sub>2</sub>  | 0.44  | 0.46  | 0.52  | 0.41  | 0.43  | 0.41  | 0.34  | 0.37  | 0.36  |
| Al <sub>2</sub> O <sub>3</sub>  | 13.19 | 13.14 | 13.17 | 11.61 | 12.95 | 12.43 | 11.19 | 11.64 | 11.33 |
| Cr <sub>2</sub> O <sub>3</sub>  | 0.00  | 0.00  | 0.00  | 0.01  | 0.00  | 0.00  | 0.00  | 0.02  | 0.00  |
| MgO   | 0.65  | 0.57  | 0.40  | 0.66  | 0.51  | 0.37  | 0.43  | 0.47  | 0.47  |
| CaO   | 3.49  | 3.38  | 3.42  | 4.14  | 3.07  | 2.90  | 3.08  | 2.97  | 3.58  |
| MnO   | 0.17  | 0.18  | 0.13  | 0.11  | 0.17  | 0.25  | 0.10  | 0.12  | 0.12  |
| FeO   | 3.74  | 3.47  | 3.90  | 4.80  | 3.72  | 4.11  | 3.17  | 3.31  | 4.38  |
| NiO   | 0.00  | 0.00  | 0.00  | 0.00  | 0.00  | 0.02  | 0.00  | 0.00  | 0.02  |
| Na <sub>2</sub> O   | 1.36  | 1.21  | 1.10  | 1.03  | 1.23  | 1.36  | 1.34  | 1.20  | 0.94  |
| K <sub>2</sub> O  | 0.70  | 0.66  | 0.47  | 0.79  | 0.77  | 0.47  | 0.90  | 0.98  | 0.74  |
| total   | 95.96 | 96.05 | 92.05 | 97.03 | 96.98 | 93.72 | 95.86 | 98.06 | 94.45 |
| CIPW norm (anhydrous norms calculated at Fe <sub>2</sub> O <sub>3</sub> /FeO=0.2) |       |       |       |       |       |       |       |       |       |
| qz  | 53.3  | 55.7  | 53.6  | 56.4  | 56.2  | 57.4  | 58.6  | 56.6  | 55.2  |
| or  | 4.3   | 4.1   | 4.8   | 4.7   | 3.0   | 5.6   | 5.9   | 4.6   | 3.0   |
| ab  | 12.0  | 10.7  | 9.0   | 10.7  | 12.3  | 11.8  | 10.4  | 8.4   | 10.1  |
| an  | 18.0  | 17.5  | 21.2  | 15.7  | 15.4  | 15.9  | 15.0  | 18.8  | 18.4  |
| hy  | 6.3   | 5.7   | 7.6   | 5.8   | 6.4   | 5.0   | 5.1   | 6.8   | 5.9   |
| c   | 4.0   | 4.5   | 1.6   | 4.7   | 4.7   | 2.5   | 3.3   | 2.6   | 5.0   |
| mt  | 1.3   | 1.2   | 1.6   | 1.2   | 1.4   | 1.1   | 1.1   | 1.5   | 1.4   |
| il  | 0.9   | 0.9   | 0.8   | 0.8   | 0.8   | 0.7   | 0.7   | 0.7   | 1.1   |
| total   | 100.1 | 100.3 | 100.2 | 100.0 | 100.2 | 100.0 | 100.1 | 100.0 | 100.1 |
| D.I.  | 69.6  | 70.4  | 67.4  | 71.8  | 71.4  | 74.9  | 74.8  | 69.7  | 68.3  |
| An%   | 60.1  | 62.1  | 70.2  | 59.4  | 55.6  | 57.4  | 59.2  | 69.1  | 64.6  |
| Mg No.  | 27.9  | 26.8  | 23.5  | 23.4  | 16.7  | 23.2  | 24.0  | 19.3  | 18.6  |

P1, 2, 4, 5, 6, 7 groundmass glass; P2(i), P5(i), P7(i) glass inclusions in orthopyroxene; D.I., An% and Mg No. calculations follow procedures in Hughes (1982). D.I., Differentiation Index.

**Table 4.** Trace element composition (ppm) of representative rhyodacitic glasses and dacite matrix, eastern Australian and Southwest Pacific examples.

| locality | Balmoral Beach eastern Australia |      |      |      | Tonga |          | Kermadec  | Lau Basin |          |
|----------|----------------------------------|------|------|------|-------|----------|-----------|-----------|----------|
|          | P2                               | P4   | P6   | P7   | Metis | Fonualei | Curtis Is | 840C-6#   | 838A-11H |
| Rb       | 1.3                              | 15   | 9.9  | 274  | 21    | 26       | 6.8       | 9.2       | 4.9      |
| Sr       | 21                               | 232  | 388  | 330  | 130   | 245      | 175       | 98        | 191      |
| Y        | 18                               | 27   | 11   | 67   | 25    | 32       | 41        | 21        | 16       |
| Zr       | 18                               | 50   | 20   | 178  | 68    | 61       | 84        | 84        | 49       |
| Nb       | 0.2                              | 1.0  | 0.7  | 11   |       |          |           | 1.5       | 0.6      |
| Ba       | 33                               | 475  | 643  | 618  | 610   | 380      | 3.45      | 153       | 56       |
| La       | 0.8                              | 3.0  | 1.9  | 45   |       | (4)      | 4.6       | 5.8       | 3.6      |
| Ce       | 2.5                              | 9.2  | 4.8  | 111  |       | (12)     | 14.4      | 16.1      | 8.4      |
| Pr       | 0.6                              | 1.5  | 1.1  | 11   |       |          |           |           |          |
| Nd       | 3.5                              | 7.1  | 4.0  | 42   |       | (9)      | 11.4      | 12.1      | 7.1      |
| Eu       | 0.3                              | 0.8  | 0.9  | 3.3  |       |          | 1.3       | 1.9       | 0.8      |
| Sm       | 1.4                              | 2.8  | 1.8  | 8.6  |       |          | 3.6       | 3.7       | 2.0      |
| Gd       | 2.2                              | 2.9  | 1.9  | 8.4  |       |          | 5.0       |           |          |
| Ho       | 0.8                              | 1.6  | 0.5  | 1.6  |       |          |           |           |          |
| Yb       | 2.2                              | 4.0  | 1.5  | 6.6  |       |          | 4.0       | 3.4       |          |
| Lu       | 0.3                              | 0.8  | 0.3  | 1.2  |       |          |           |           |          |
| Hf       | 0.6                              | 2.9  | 0.7  | 4.4  |       |          |           |           |          |
| Pb       | 0.6                              | 8.6  | 4.7  | 85   |       |          | 5.1       |           |          |
| Th       | 0.1                              | 0.6  | 0.4  | 22   |       | (0.7)    | 2.1       |           |          |
| U        | 0.0                              | 0.9  | 0.7  | 8.3  |       | (0.4)    | 0.8       |           |          |
| La/Yb    | 0.36                             | 0.75 | 1.3  | 6.8  |       |          | 1.15      | 1.71      | 0.23     |
| Y/Zr     | 1.00                             | 0.54 | 0.55 | 0.38 | 0.37  | 0.52     | 0.49      | 0.25      | 0.33     |
| Rb/Zr    | 0.07                             | 0.30 | 0.50 | 1.54 | 0.31  | 0.43     | 0.08      | 0.11      | 0.10     |
| Ba/La    | 41.3                             | 158  | 338  | 13.7 |       | 95.0     | 75.0      | 26.4      | 15.6     |
| Sr/Nd    | 6.0                              | 32.7 | 97.0 | 7.86 |       | 27.2     | 15.4      | 8.10      | 26.9     |
| Ba/Th    | 330                              | 792  | 1608 | 28.1 |       | 543      | 164       |           |          |
| Ba/Sr    | 1.57                             | 2.05 | 1.66 | 1.87 | 4.69  | 1.55     | 1.97      | 1.56      | 0.29     |
| Ba/Rb    | 25.4                             | 31.7 | 64.9 | 2.26 | 29.0  | 14.6     | 50.7      | 16.6      | 11.4     |
| Rb/Sr    | 0.06                             | 0.06 | 0.03 | 0.83 | 0.16  | 0.11     | 0.04      | 0.09      | 0.03     |

P2, P4, P6, P7 this work; Metis Shoal and Fonualei, Tonga, from Ewart *et al.* (1973) and Ewart & Hawkesworth (1987); Curtis Island, Kermadec (from Ewart *et al.*, 1977); Lau Basin (from Clift & Vroon, 1996).

**Table 5.** Mineral and glass compositions and calculated bulk compositions for main layer pumices (P1, P2), Balmoral Beach site.**Pumice P1 (5% xenocrysts/phenocrysts, 20% glass)**

| wt%                            | mineral component compositions |       |      |      |      |      |      |      | glass comp | bulk comp |
|--------------------------------|--------------------------------|-------|------|------|------|------|------|------|------------|-----------|
|                                | Plag1                          | Plag2 | Cpx  | Opx  | Ox1  | Ox2  | O11  | O12  |            |           |
| SiO <sub>2</sub>               | 50.8                           | 56.9  | 52.6 | 51.8 | 0.1  | –    | 38.9 | 40.5 | 72.2       | 67.0      |
| TiO <sub>2</sub>               | –                              | –     | 0.2  | 0.2  | –    | 47.6 | –    | –    | 0.4        | 0.7       |
| Al <sub>2</sub> O <sub>3</sub> | 30.9                           | 26.7  | 2.7  | 0.7  | –    | 0.2  | –    | –    | 13.2       | 13.7      |
| MgO                            | –                              | –     | 16.8 | 18.6 | –    | 2.0  | 42.6 | 49.2 | 0.7        | 2.2       |
| CaO                            | 14.4                           | 9.9   | 23.2 | 1.6  | 0.1  | –    | 0.2  | 0.3  | 3.5        | 5.2       |
| MnO                            | –                              | –     | 0.1  | 1.4  | 0.2  | 1.1  | 0.4  | 0.1  | 0.2        | 0.2       |
| FeO total                      | 0.4                            | 0.4   | 4.1  | 25.8 | 80.8 | 47.7 | –    | –    | 3.7        | 5.4       |
| Na <sub>2</sub> O              | 3.4                            | 6.1   | 0.1  | –    | –    | –    | –    | –    | 1.4        | 1.5       |
| K <sub>2</sub> O               | –                              | 0.1   | –    | –    | –    | –    | –    | –    | 0.7        | 0.6       |
| % of rock                      | 2.25                           | 0.25  | 1.0  | 0.75 | 0.4  | 0.1  | 0.2  | 0.05 | 20.0       | 25.0      |

**Pumice P2 (4% xenocrysts/phenocrysts, 20% glass)**

| wt%                            | mineral component compositions |      |      |      |      |      | glass comp | bulk comp |
|--------------------------------|--------------------------------|------|------|------|------|------|------------|-----------|
|                                | Plag                           | Cpx1 | Cpx2 | Opx  | Ox   | Ol   |            |           |
| SiO <sub>2</sub>               | 52.7                           | 51.3 | 52.6 | 51.8 | 0.1  | 41.3 | 73.0       | 69.0      |
| TiO <sub>2</sub>               | –                              | 0.3  | 0.1  | 0.2  | 14.4 | –    | 0.5        | 0.6       |
| Al <sub>2</sub> O <sub>3</sub> | 29.5                           | 1.0  | 2.6  | 0.5  | 2.2  | –    | 13.1       | 13.5      |
| MgO                            | –                              | 11.8 | 17.1 | 18.8 | 1.3  | 42.4 | 0.6        | 2.0       |
| CaO                            | 13.0                           | 19.1 | 23.2 | 1.6  | –    | 0.2  | 3.4        | 4.3       |
| MnO                            | –                              | 0.9  | –    | 1.4  | 0.8  | 1.2  | 0.2        | 0.3       |
| FeO total                      | 0.6                            | 15.4 | 3.9  | 25.6 | 79.9 | 15.8 | 3.5        | 5.3       |
| Na <sub>2</sub> O              | 4.3                            | 0.2  | 0.1  | –    | –    | –    | 1.2        | 1.4       |
| K <sub>2</sub> O               | –                              | –    | –    | –    | –    | –    | 0.7        | 0.6       |
| % of rock                      | 2.0                            | 0.3  | 0.1  | 1.2  | 0.2  | 0.2  | 20.2       | 24.0      |

**Table 6.** Comparative bulk and glass compositions, Australia/Southwest Pacific dacites. ND, not determined.

| wt%   | Balmoral<br>eastern Australia <sup>1</sup> |         | Metis Shoal<br>Tonga <sup>2</sup> |         | Herald Cays<br>eastern Australia <sup>3</sup> |         | Fonualei<br>Tonga <sup>2</sup> |          |
|---|--|---------|-----------------------------------|---------|---|---------|--------------------------------|----------|
|   | (bulk)                                     | (glass) | (bulk)                            | (glass) | (dark)  | (light) | (bulk)                         | (matrix) |
| SiO <sub>2</sub>  | 67.0                                       | 72.2    | 63.7                              | 73.6    | 67.2  | 73.5    | 65.6                           | 73.2     |
| TiO <sub>2</sub>  | 0.5  | 0.4     | 0.4                               | 0.5     | 0.6   | 0.6     | 0.6                            | 0.4      |
| Al <sub>2</sub> O <sub>3</sub>  | 13.7                                       | 13.2    | 12.4                              | 12.3    | 12.1  | 11.9    | 14.0                           | 11.8     |
| Fe <sub>2</sub> O <sub>3</sub>  |  |         | 1.4                               | 1.3     | 0.5   | 0.8     | 2.1                            | 1.0      |
| FeO   | 5.4t                                       | 3.7t    | 5.2                               | 2.7     | 8.5   | 4.8     | 6.1                            | 4.3      |
| MnO   | 0.2  | 0.2     | 0.1                               | 0.1     | 0.1   | –       | 0.2                            | 0.1      |
| MgO   | 2.2  | 0.7     | 5.1                               | 1.1     | 1.3   | 0.6     | 1.4                            | 0.7      |
| CaO   | 5.2  | 3.5     | 7.0                               | 3.6     | 5.6   | 3.8     | 5.7                            | 3.8      |
| Na <sub>2</sub> O   | 1.5  | 1.4     | 2.6                               | 3.2     | 2.6   | 2.8     | 3.0                            | 3.2      |
| K <sub>2</sub> O  | 0.6  | 0.7     | 0.9                               | 1.5     | 0.6   | 0.8     | 1.1                            | 1.4      |
| P <sub>2</sub> O <sub>5</sub>   | –  | –       | 0.1                               | 0.1     | 0.2   | 0.1     | 0.2                            | 0.2      |
| H <sub>2</sub> O±   | ND   | ND      | 0.9                               | 0.1     | 0.3   | 0.5     | ND                             | ND       |
| total   | 96.5                                       | 96.0    | 99.8                              | 100.1   | 99.6  | 100.2   | 100.0                          | 100.0    |
| CIPW anhydrous norms (calculated at Fe <sub>2</sub> O <sub>3</sub> /Fe <sub>2</sub> O <sub>3</sub> + FeO = 0.2); t = total FeO. |  |         |                                   |         |   |         |                                |          |
| q   | 40.1                                       | 52.9    | 22.6                              | 38.7    | 33.3  | 42.9    | 27.0                           | 38.6     |
| or  | 3.7  | 4.3     | 5.4                               | 8.9     | 3.6   | 4.7     | 6.5                            | 8.3      |
| ab  | 13.2                                       | 12.3    | 22.3                              | 27.1    | 22.2  | 23.8    | 25.4                           | 27.1     |
| an  | 26.8                                       | 18.1    | 19.7                              | 14.8    | 19.7  | 17.6    | 21.5                           | 13.7     |
| di  |  |         | 12.0                              | 2.1     | 6.0   | 0.6     | 4.7                            | 3.3      |
| hy  | 12.4                                       | 6.5     | 14.9                              | 6.0     | 11.0  | 7.3     | 10.7                           | 6.2      |
| mt  | 1.8  | 1.2     | 2.1                               | 1.3     | 2.9   | 1.8     | 2.6                            | 1.7      |
| il  | 1.0  | 0.8     | 0.8                               | 1.0     | 1.2   | 1.1     | 1.1                            | 0.8      |
| c   | 1.2  | 3.9     |                                   |         |   |         |                                |          |
| ap  |  |         | 0.2                               | 0.2     | 0.5   | 0.2     | 0.5                            | 0.5      |
| D.I.  | 57.0                                       | 69.6    | 50.3                              | 50.3    | 59.0  | 71.4    | 58.9                           | 73.9     |
| An%   | 67.0                                       | 59.4    | 47.0                              | 47.0    | 47.1  | 42.5    | 45.8                           | 33.6     |
| Mg No.  | 47.6                                       | 29.7    | 63.8                              | 63.8    | 24.5  | 19.5    | 28.1                           | 23.1     |
| Na <sub>2</sub> O/K <sub>2</sub> O  | 2.5  | 2.0     | 2.9                               | 2.1     | 4.3   | 3.5     | 2.7                            | 2.3      |

<sup>1</sup> from Table 4, this work.<sup>2</sup> after Ewart *et al.* (1973).<sup>3</sup> after Bryan (1968).